This is the accepted manuscript of the article that appeared in final form in **Dyes and Pigments** 170 : (2019) // Article ID 107545, which has been published in final form at https://doi.org/10.1016/j.dyepig.2019.107545. © 2019 Elsevier under CC BY-NC-ND license (http://creativecommons.org/licenses/by-nc-nd/4.0/)

A General Modular Approach for the Solubility Tagging of BODIPY Dyes

Alberto Blázquez-Moraleja, Delia Álvarez-Fernández, Ruth Prieto Montero, Inmaculada García-Moreno, Virginia Martínez-Martínez, Jorge Bañuelos Prieto, Inés Sáenz-de-Santa-María, María D. Chiara, and Jose Luis Chiara

Dyes and Pigments 2019, 170, 107545

https://doi.org/10.1016/j.dyepig.2019.107545

A General Modular Approach for the Solubility Tagging of BODIPY Dyes

Alberto Blázquez-Moraleja, Delia Álvarez-Fernández,† Ruth Prieto Montero,† Inmaculada García-Moreno, Virginia Martínez-Martínez,* Jorge Bañuelos Prieto, Inés Sáenz-de-Santa-María, María D. Chiara, and Jose Luis Chiara*

A. Blázquez-Moraleja, D. Álvarez-Fernández, Dr. J. L. Chiara
Instituto de Química Orgánica General, IQOG-CSIC, Juan de la Cierva 3, 28006 Madrid, Spain
E-mail: jl.chiara@csic.es

R. Prieto Montero, Dr. V. Martínez-Martínez, Dr. J. Bañuelos Prieto
Departamento de Química Física, Universidad del País Vasco-EHU, Facultad de Ciencias y Tecnología, Apartado 644, 48080 Bilbao, Spain
E-mail: virginia.martinez@ehu.eus

Prof. I. García-Moreno
Instituto Química-Física "Rocasolano", IQFR-CSIC, Serrano 119, 28006 Madrid, Spain

Dr. I. Sáenz-de-Santa-María, Dr. M. D. Chiara
Institute of Sanitary Research of Asturias, Institute of Oncology of Asturias (IUOPA), CIBERONC, Universidad de Oviedo, Hospital Central de Asturias, 33011 Oviedo, Spain

†These authors have contributed equally to this work

Keywords: fluorescent dyes, BODIPYs, aqueous solubility, imaging agents, density functional calculations

The authors have no competing interests to declare.

Abstract

We describe a general and practical strategy for the direct one-step incorporation of a tunable solubility module at the boron atom of *F*-BODIPY dyes. The tethering reaction uses easy-to-handle reagents, has broad functional group compatibility and proceeds under mild conditions without requiring any pre-functionalization of the starting *F*-BODIPY to yield the solubility-tagged *O*-BODIPY derivative in 51-86% yield. The module can be introduced at the end of the synthetic route without perturbing the fluorophore scaffold, thus minimizing difficulties in product isolation. Its orthogonal geometrical arrangement with respect to the plane of the

BODIPY chromophore hampers intermolecular aggregation processes that quench fluorescence, while the covalent attachment to the boron atom has a minimal effect on the absorption properties. Fully water-soluble and hydrolytically stable BODIPYs were prepared by incorporating either neutral (tetra- and octaethylene glycol chains) or zwitterionic (sulfobetaine) hydrophilic tags in the module. The new dyes are valuable live cell imaging probes that ameliorate the undesired partitioning into lipophilic compartments that is often observed for standard BODIPYs. This strategy can be readily adapted to the general and highly practical post-synthetic introduction of new functionalities into *F*-BODIPY dyes, including phase-tagging, by appropriately choosing the nature of the chemical tags attached to the module.

1. Introduction

The expanding development of chromogenic and fluorogenic probes for practical applications in the study of biosystems critically depends on the facility to post-synthetically introduce diverse functionalities that improve the analytical and physicochemical properties of the probe without significantly affecting its photophysical properties. Among commonly used dyes for biological studies, BODIPYs outstand for their fascinating chemical, electronic, and photophysical features, comprising large molar absorption coefficients, sharp fluorescence emissions with high fluorescence quantum yields, excellent photostability, and broad chemical versatility.[1] However, due to its inherent hydrophobic nature, the standard BODIPY chromophore has also serious drawbacks for its application in biological research, such as a very low solubility in aqueous media and a tendency to form aggregates.[2] As a consequence, BODIPYs often partition into lipophilic compartments of cells resulting in nonspecific staining of biomembranes and/or cell organelles, which can seriously bias the cellular distribution of labeled small molecules. Likewise, they also tend to embed into hydrophobic pockets[3] when conjugated to biomolecules, which may affect the biological function of the bioconjugate.

Different approaches have been developed along the last decade to improve water solubility and minimize aggregation of BODIPY dyes, which include the introduction of ionizable or permanently charged hydrophilic groups, such as anionic carboxylic,[4] phosphonic[4b,4c,5] and sulfonic acid salts,[4c,6] cationic phosphonium[7] and ammonium groups,[4c,8] and zwitterionic sulfobetaines,[4,6e,9] or grafting the fluorophore to hydrophilic (bio)/mono-/oligo-/polymers, such as carbohydrates,[8c,10] peptides,[11] oligonucleotides,[12] and mono-/oligoethylene glycols.[13] While significantly improving water solubility, the ionic character and/or large size of the solubilizing groups often impair membrane permeability, which limit the practical application of the fluorescent tag in live cell and *in vivo* imaging. In addition, most of these approaches implement multistep synthetic routes to introduce the desired water-solubilizing groups, which have to be masked during the synthesis to avoid troublesome purifications and/or prevent cross reactivity.

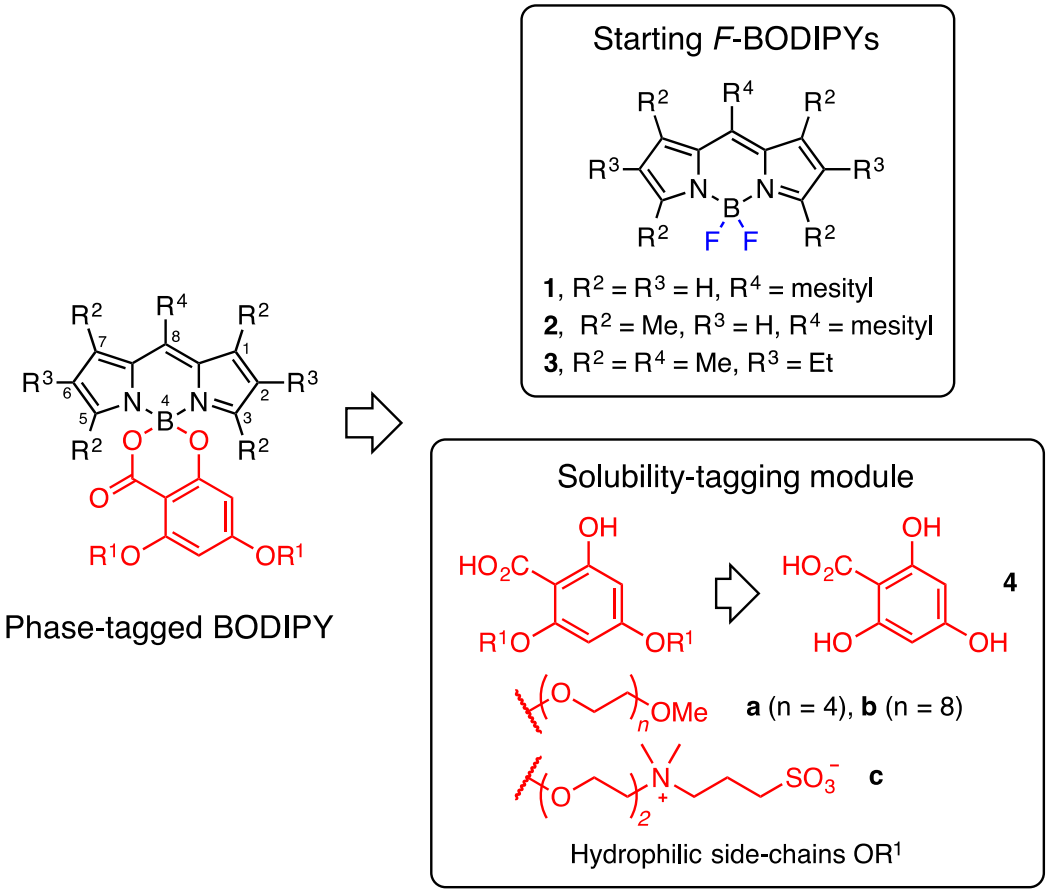

Figure 1. General modular approach for the solubility-tagging of *F*-BODIPYs described in this work.

We describe herein a general and practical strategy for the efficient one-step, post-synthetic introduction of a finely tunable solubility module into *F*-BODIPY dyes (Figure 1). In our strategy, the solubility module can be directly introduced at the end of the synthetic route without perturbing the fluorophore scaffold, thus minimizing difficulties in product isolation. To this end, we selected a covalent functionalization reaction with a broad functional group compatibility that proceeds under mild conditions and in high yield without requiring any pre-functionalization of the chromophore. Such a reaction is the basis of our recently described one-step synthesis of *O*-BODIPYs with a rigid *B*-spiranic 4,4-diacyloxyl or 4-acyloxyl-4-alkoxyl substitution pattern starting from the corresponding *F*-BODIPYs.[14] Our original protocol allows the direct modification of known *F*-BODIPY dyes at the boron atom via an efficient F-to-O exchange reaction that uses simple reagents and conditions, providing an easy access to diversely functionalized mono-[14a] and bichromophoric[14b] *O*-BODIPYs. In addition, the conformational rigidity of the resulting *B*-spiranic system boosts fluorescence quantum yield and photochemical stability, while the orthogonal disposition of the *B*-chelated di-O-substituent with respect to the mean plane of the boradiazaindacene framework hinders intermolecular π-stacking aggregation of the chromophores, which impede the formation of H-dimers that strongly quench fluorescence. Moreover, substitution at boron usually has a minimal effect on the absorbance and emission properties of the BODIPY chromophore. Starting from known *F*-BODIPYs **1**-**3**, we have validated our strategy by designing a rigid water-solubilizing module based on 2,4,6-trihydroxybenzoic acid (phloroglucinol carboxylic acid, **4**) as the core, incorporating two identical hydrophilic side chains of different nature, neutral or zwitterionic, to promote water solubility, thus allowing the use of our dyes in aqueous biological environments (Figure 1).

2. Results and Discussion

2.1. Synthetic approach to solubility-tagged BODIPYs. The synthesis route to the different solubility-tagged modules and the final tagged water-soluble BODIPYs is shown in Scheme 1. First, the salicylic acid portion of **4**, which will be covalently attached to boron in the final dye, was protected as an acetonide ester **5** following a literature procedure.[15] The hydrophilic tags were then introduced in one step using a Mitsunobu protocol[15,16] to afford the protected modules **6a-c**. As hydrophilic tags, we have chosen two neutral oligoethylene glycol chains of different lengths, based on commercially available tetra- and octaethylen glycol monomethyl ether (R^1O = **a** and **b**, respectively), and a zwitterionic (sulfobetaine) chain (R^1O = **c**, Figure 1) that was readily prepared from 2-[2-(dimethylamino)ethoxy]etanol and propane sultone using a modification of a described procedure.[17] Removal of the acetonide protecting group under carefully controlled hydrolytic conditions,[18] afforded the final hydrophilic modules **7a**-**c** ready for tethering to *F*-BODIPYs. As commented above, these modules were then directly incorporated into the *F*-BODIPYs **1**-**3** included in this work, using our recently described one-step protocol.[14] Thus, a stoichiometric mixture of *F*-BODIPY and the corresponding module **7a**-**c** in anhydrous MeCN was heated under microwave irradiation (50-120 °C, 0.75-2 h) in the presence of an excess of TMSCl (20-50 equiv) to afford the targeted water-soluble *O*-BODIPYs **1a**-**b**, **2a**-**c**, and **3a**-**c** in moderate to good yield (51-86%), after solvent removal and chromatographic purification (Scheme 1). This F-to-O exchange method uses an easy-to-handle and volatile reagent, avoids aqueous work-up (the TMSCl reagent and the corresponding TMSF only by-product are both volatile) and is experimentally simpler, more efficient, and yields cleaner reaction crudes than all previously reported methodologies to prepare *O*-BODIPYs.[13e,19]

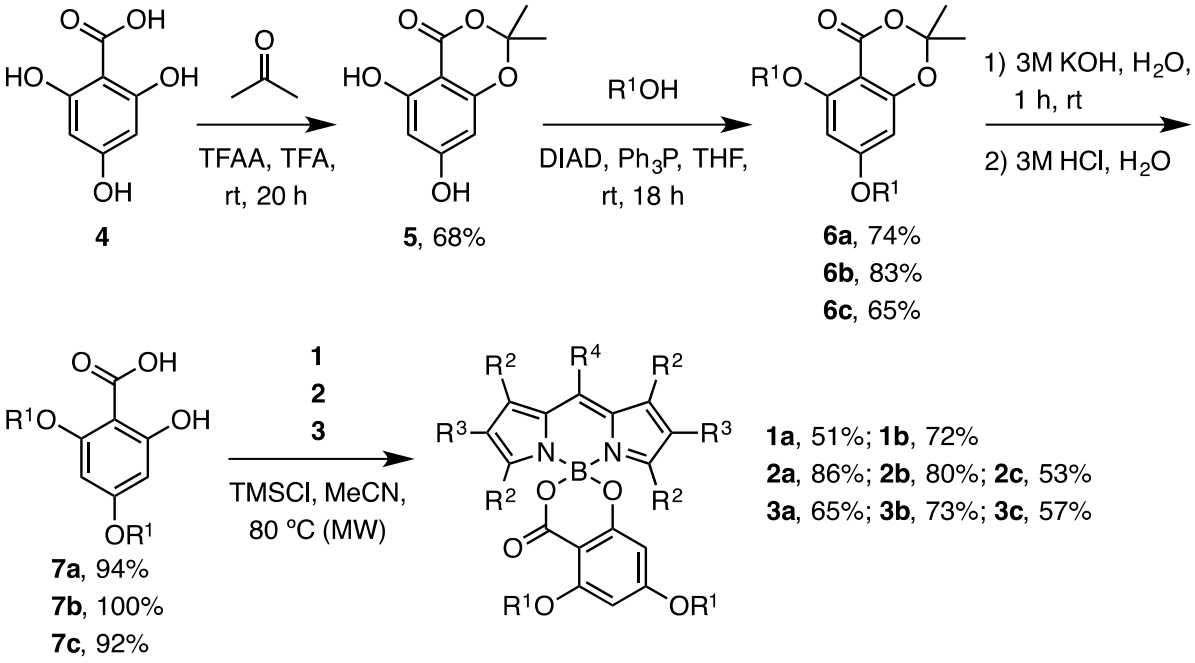

Scheme 1. Synthesis of the water-solubilizing modules and the final water-soluble BODIPYs (see Figure 1 for the chemical structures of the R substituents).

2.2. Photophysical characterization.

A comprehensive computationally-aided photophysical study was performed on the newly synthesized *O*-BODIPYs. At a first sight, the solubility-tagged module linked to the boron atom of the BODIPY skeleton should not significantly affect the photophysics of the new dyes.[14a,20] Indeed, in related *O*-BODIPYs the presence of different spiranic rings centered at the boron bridge neither alters the absorption profile nor the fluorescence signatures, following thereby a photophysical behavior similar to their respective parent *F*-BODIPY precursors.[14a,,19d,21] Strikingly, upon addition of the hydrophilic chains to the phenyl group of the solubility module some photophysical properties become strongly dependent on both the substitution pattern of the chromophoric core and the solvent polarity. The hydrophilic chains did not alter the absorption properties (band-shape, absorption coefficient and maximum wavelength) nor their typical solvent dependence, hypsochromically shifting the maximum wavelength and reducing the molar extinction coefficient on increasing solvent polarity.[14a,19d,21] However, they induced a dramatic effect on the fluorescent emission of the new dyes (Tables 1 and S1). In

particular, dyes **1a**-**b** exhibited low fluorescence quantum yields and short lifetimes, which are far from the typical values of similar 8-mesityl substituted *F*-BODIPYs (Table 1 and S1).[22]

Table 1. Photophysical properties of dyes **1b, 2b** and **3b** in different solvents.[a] The photophysical data for the other dyes are collected in Tables S1-S3.

Dye	Solvent	λ_{ab}[b] (nm)	ε_{max}[c] (10^4 M^{-1} cm^{-1})	λ_{fl}[d] (nm)	ϕ_{flu}[e]	τ[f] (ns)
1b	$CHCl_3$	507.0	5.8	521.0	0.06	0.49
	EtOH	505.0	5.1	514.5	0.02	0.11
	H_2O	503.0	4.0	514.0	<0.01	<0.15
2b	$CHCl_3$	507.0	7.8	515.5	0.86	5.82
	EtOH	504.0	6.9	514.5	0.79	6.60
	H_2O	502.0	4.2	511.5	0.78	6.40
3b	$CHCl_3$	527.0	6.2	547.0	0.73[g]	6.85
	EtOH	523.0	4.5	545.5	0.72[g]	7.28
	H_2O	520.0	4.9	540.0	0.71[g]	7.77

[a]Dye concentration: 2×10^{-6} M. [b]Absorption peak wavelength. [c]Molar extinction coefficient at peak. [d]Fluorescence peak wavelength, upon excitation at 490 nm. [e]Using quantum yield of PM546 (ϕ_{fl} = 0.91) in cyclohexane as reference. [f]Fluorescence lifetime. [g]Using quantum yield of PM567 (ϕ_{fl} = 0.84) in ethanol as reference. The fluorescence data are recorded in right angle using a 1 cm optical path cell.

Since the low emission efficiency of dyes **1a** and **1b** could not be attributed to the molecular flexibility of the 8-aryl substituent,[22] we hypothesized that its fluorescent behavior may be related to the high electron density of the substituent grafted at the boron center (a phenyl group decorated with three electron-donor oxygen atoms). Dramatic fluorescence quenching in *O*-BODIPYs has been already reported upon introduction of a spiranic ring at the boron bridge (e.g. catechol or binol).[23] Such derivatives are weakly emissive due to the activation of intramolecular charge transfer (ICT) processes, which could eventually evolve into a photoinduced electron transfer (PET) as the main non-radiative deactivation channel.[23]

Trying to confirm this hypothesis, we carried out DFT atomistic simulations (B3LYP/6-311+G*) of dye **1a** and its methylated analog **2a** as representative compounds (Figure 2). The HOMO–1 of the non-methylated BODIPY **1a**, almost entirely located on the pendant aromatic moiety grafted at the boron atom, is energetically very close to the HOMO (just 0.08 eV below), which is completely located on the dipyrrin system. Such energetic distribution of molecular orbitals envisaged the ability of the electron-rich salicylic system to effectively induce an intramolecular charge transfer (ICT) process and even enable a reductive photoinduced electron transfer (PET) upon excitation. Thus, upon the photoinduced promotion of an electron from the HOMO to the LUMO, an electron transfer from the low-lying HOMO–1 to the semi-vacant HOMO is thermodynamically feasible. Such a reductive PET from the spiranic group grafted at boron to the BODIPY core avoids radiative deactivation from the LUMO back to the HOMO, thus explaining the almost negligible fluorescence emission of **1a.** The presence of alkyl groups on the chromophoric core of **2a**, drastically changes the energetic arrangement of the molecular orbitals. Thus, with respect to dye **1a**, the inductive electron-donor ability of the methyl groups in **2a** increases the energy of the HOMO and LUMO orbitals (by ca. 0.56 eV and ca. 0.35 eV, respectively) without energetically altering the HOMO–1. Consequently, the energy gap between the frontier orbitals HOMO–1 and HOMO (0.58 eV) becomes 7-fold higher than in the non-methylated counterpart **1a,** thus hampering an effective PET process and thereby allowing the fluorescence emission of the BODIPY. Therefore, tetramethylation of the BODIPY scaffold reduces the electron-acceptor character of the chromophoric core making thermodynamically unfeasible any ICT process induced by the functionalization at its boron bridge. Thus, the bright fluorescence emission and long excited-state lifetimes of typical BODIPYs are recovered in dyes **2a**-**c** (Tables 1 and S2).[14a,19d,20-22] In the same manner, the electron-donor character of the ethyl groups additionally grafted at the C-2 and C-6 positions of BODIPYs **3a**-**c** further reduces the probability of an ICT process, allowing these dyes to emit highly efficient fluorescence with

elongated lifetimes regardless of the length and nature of the hydrophilic chains and the solvent polarity (Tables 1 and S3).

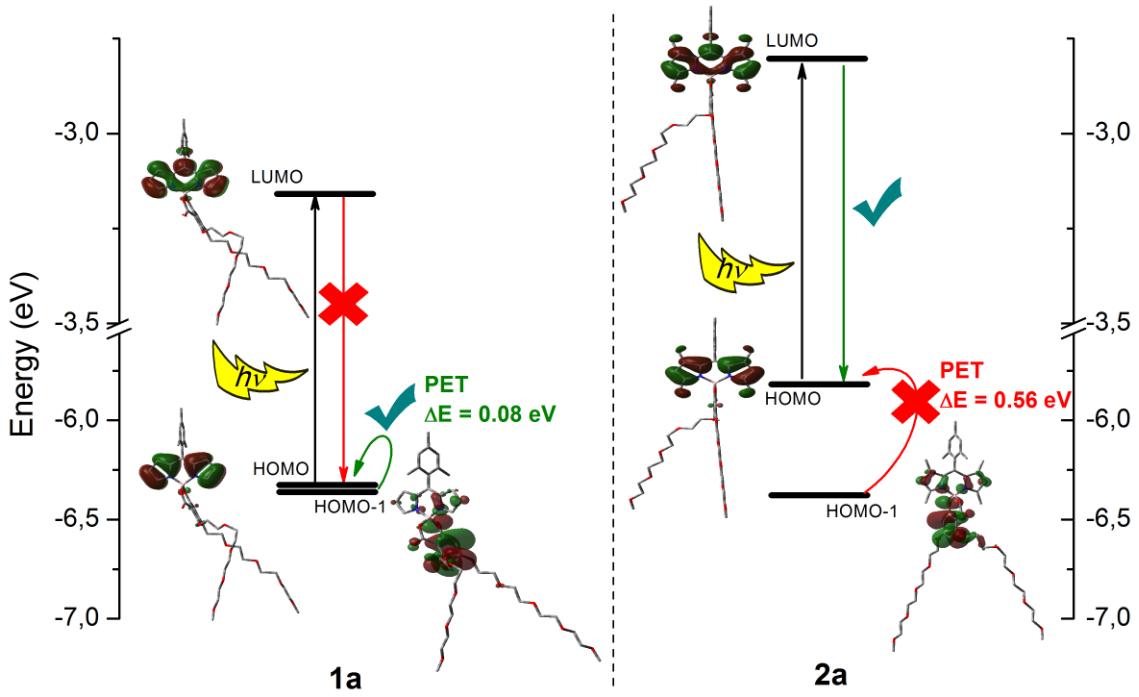

Figure 2. Calculated (B3LYP/6-311+G*) energetic arrangement of the frontier molecular orbitals of the non-methylated BODIPY **1a** and its tetramethylated analog **2a.**

In addition, the alkyl substituents on the BODIPY core may also play a major role in controlling intermolecular interactions. The capability of the new dyes to avoid non-fluorescent aggregation in water would impel their application in biological settings, since fluorescent probes are typically used in concentrations higher than 2 μM. To understand the intermolecular interactions of dyes **2a-c** and **3a-c** in aqueous media, the photophysical studies were also performed at increasing concentrations of dye in water (see Experimental Section for details). The fluorescence quantum yields of **2a-c** and **3a-c** (approximate values at the highest concentrations) were not significantly affected by augmenting dye concentration from 2×10^{-6} M to 10^{-4} M, which emphasized the absence of aggregates and the enhanced water solubility of the new dyes (Tables 2, S4 and S5). A further increase in concentration led to the gradual quenching of the emission efficiency, which could be ascribed, at least to some extent, to the

strengthening of reabsorption/reemission processes (Table S4 and S5).[24] In addition, growing concentrations markedly changed the spectral profiles depending on the substitution pattern of the chromophoric backbone. In the case of **2a**-**c**, an increase of dye concentration in water produced a gradual broadening and a slight red-shift of the absorption spectra, without entailing neither the growth of vibronic shoulders nor the appearance of new bands (Figure 3). Likewise, unusual features emerged in the emission spectra, with the intensity of the long-wavelength shoulder growing with dye concentration (Figure 3) until reaching or even exceeding the intensity of the main fluorescence band (Figure S3). Interestingly, the fluorescence lifetime was never significantly shortened in highly concentrated solutions with respect to that recorded in diluted solutions (Tables 2 and S4). This spectral behavior is fingerprint of short-range intermolecular interactions, likely excimer-like species and/or J-type aggregates.[14a]

Table 2. Dependence of the fluorescence quantum yield and lifetime of new derivatives **2c**[a] and **3c**[b] on dye concentration in water. The data for the other dyes are collected in Tables S4-S5.

	Dye **2c**				Dye **3c**			
$[c]$x10^4 (M)	ϕ[c]	ϕ[d]	τ (ns)[c]	τ (ns)[d]	ϕ[c]	ϕ[d]	τ (ns)[c]	τ (ns)[d]
0.02	0.86		5.99	-	0.78	-	7.25	-
0.05	0.85		6.09	-	0.78	-	7.27	-
0.1	0.86		6.19	-	0.78	-	7.36	-
0.2	0.85		6.36	-	0.76	-	7.49	-
0.3	0.83		-	-	0.78	-	7.70	-
0.7	0.87		-	-	-	-	-	-
0.9	-		-	-	0.68	0.77	7.88	-
1.6	0.45	0.58	6.76	6.25	0.35	0.48	8.22	7.48
2.3	-	-	-	-	0.22	0.34	8.24	7.47
3.5	0.19	-	-	6.47	0.06	0.24	-	7.21
7.0	-	-	-	-	0.01	0.09	-	-

[a] Upon excitation at 490 nm and using PM546 (ϕ_{Fl} = 0.91) in cyclohexane as reference. [b] Upon excitation at 490 nm and using PM567 (ϕ_{Fl} =0.84) in ethanol as reference. [c,d] Evaluated under front-face configuration using 1 and 0.1 mm optical path cuvette, respectively.

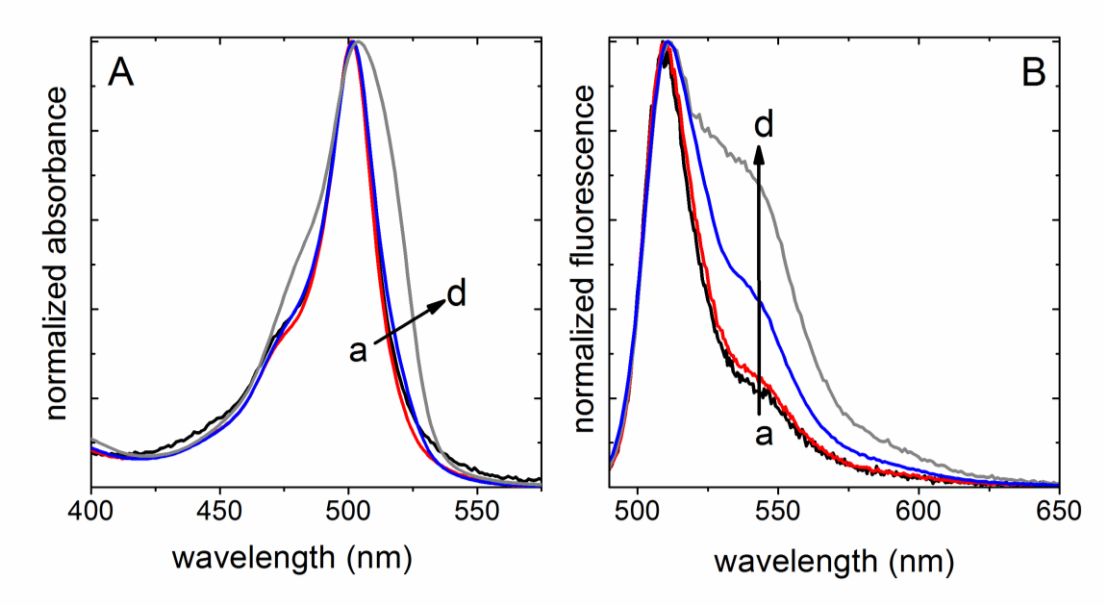

Figure 3. Height-normalized absorption (A) and emission (B) spectra of compound **2c** in water at different concentrations: a) 2.0×10^{-6} M (1cm); b) 1.0×10^{-5} M (1mm); c) 1.7×10^{-4} M (0.1mm); d) 3.4×10^{-4} M (0.1mm). The corresponding spectra for **2a-b** dyes are collected in Figures S1 and S2.

In contrast to **2a**-**c**, the absorption spectra of **3a**-**c** are strongly dependent on dye concentration (>10^{-4} M), with the vibronic shoulder placed at 490 nm growing with concentration until reaching the intensity of the main absorption band centered at 520 nm (Figure 4). Conversely, the emission spectral profile of dyes **3a**-**c** remained roughly unchanged except for a decrease of the fluorescent intensity and a slight red-shift of the main fluorescence band. This photophysical behavior (Tables 2 and S5) is indicative of not emissive H-type intermolecular interactions, which efficiently quench the fluorescence emission. The more planar structure of the boradiazaindacene unit in dyes **3a**-**c** allows an effective intermolecular π-stacking arrangement of the chromophores at high concentrations favored by the low steric hindrance of the 8-methyl group as compared to the orthogonally oriented 8-mesityl group in dyes **2a**-**c**. Thus, compounds **2a**-**c** displayed higher fluorescence quantum yields and shorter lifetimes than dyes **3a**-**c** regardless of dye concentration and solvent polarity.

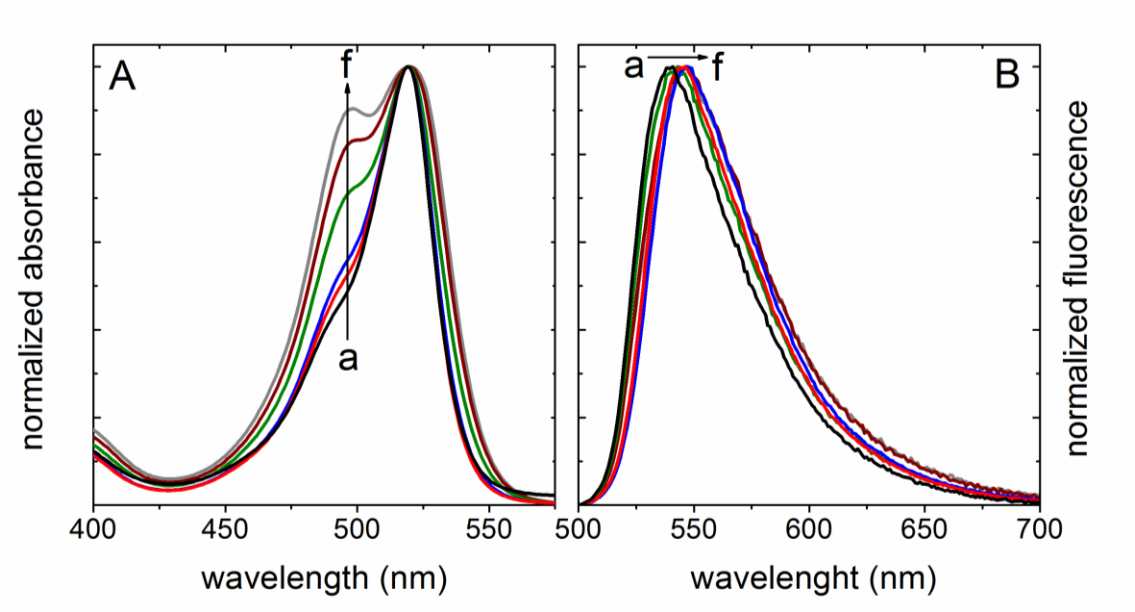

Figure 4. Height-normalized absorption (A) and emission (B) spectra for compound **3c** in water at different concentrations: a) 2.2×10^{-5} M; b) 1.6×10^{-4} M, recorded in 1-mm optical path cuvette; c) 2.3×10^{-4} M; d) 3.9×10^{-4} M; e) 6.8×10^{-4} M; f) 7.4×10^{-4} M, recorded in 0.1 mm optical path cuvette. The corresponding spectra for **3a-b** dyes are collected in Figures S3 and S4.

2.3. Solubility, chemical stability and lipophilicity.

For their intended use in live cell imaging, we have studied the solubility, stability in water, and lipophilicity of the tagged dyes. All these new BODIPYs were completely soluble in water at 10^{-4} M, which is well above the maximum typically required for cell microscopy studies. As a representative example, compound **3b** was very soluble in water with a determined maximum solubility of 10.0 ± 0.1 mM at room temperature. As expected, the di-charged sulfobetaine derivatives **2c** and **3c** were even more water-soluble, but maximum solubility values could not be reached in this case due to lack of sufficient material. In comparison, compounds **1a**, **2a** and **3a**, with the smallest neutral solubility tag, required co-addition of DMSO to fully dissolve in water in the millimolar range (see below). Thus, our modular one-step approach allows to fine tune the solubility properties of the attached BODIPY dye by a simple and efficient postsynthetic transformation.

Since the new tagged dyes contain two potentially labile B—O bonds connecting the fluorophore to the solubility module, we also monitored their chemical stability in aqueous media. Thus, we studied the evolution of BODIPYs **1a**, **2a** and **3a**, a set of dyes sharing the same solubility module, under neutral aqueous conditions (10 mM solution in 1:1 D_2O/DMSO-d_6, at room temperature) using ^{1}H NMR. The compounds were completely stable under the tested conditions with no trace of hydrolysis products being observed in the ^{1}H NMR spectra of the aged solutions even after 30 days at room temperature. For their intended application in cell microscopy, we have also studied the stability under simulated physiological conditions (cell culture medium with 10% fetal bovine serum, pH 7.4) and in phosphate buffered saline at pH 6.0 and 8.0, at room temperature, using again BODIPY **3b** as representative example. No changes in absorbance nor lineshape were observed in the UV-visible spectra of the corresponding solutions after monitoring for 7 days under these conditions (see Figures S5-S7, Supplementary Material), attesting to the very high chemical stability of these BODIPYs in the most relevant aqueous media used in biological studies. The high stability towards hydrolysis observed for these new BODIPYs probably results from the bidentate covalent binding of the salicylic module to the boron atom of the dye.

To better understand transmembrane transport and distribution of the new dyes between aqueous and hydrophobic subcellular compartments, we also assessed their lipophilicity (expressed by log *P*). Due to the limiting amount of sample, we employed the reversed-phase high-performance liquid chromatography (RP-HPLC) method with a C18 analytical column (Table 3 and Figure S8) to determine log *P*.[4d,25] The log *P* values measured for the new series of BODIPYs (log *P* = –1.51 to 4.22) fit the range of biological applications defined by Lipinski (log $P \leq 5$)[26] and were also approximately within the same range reported for other water-soluble BODIPY dyes (log *P* = –0.3 to 4.5).[4d,13e,27] For the same starting BODIPY, lipophilicity decreased with increasing aqueous solubility in the order: **a** (tetraethylene glycol chains) > **b** (octaethylene glycol chains) > **c** (sulfobetaine chains), as generally expected. For the

same solubility tag, lipophilicity decreased in the order: **2** > **3** > **1** for each **a**-**c** series of compounds, which is the same order theoretically predicted for the parent *F*-BODIPYs (CLogP = 7.56, 7.00, and 5.17, respectively, calculated with ChemBioDraw).

Table 3. Retention factors and partition coefficients of selected reference compounds used for calibration and the new BODIPY dyes.[a)]

Compound	**Retention factor**[b,c] ***k*/log *k***	**log *P***
2,6-di-tert-butyl-4-methylphenol	10.16/1.01	5.4
Diphenylmethane	3.09/0.49	4.1
1,2-Dicholorobenzene	2.09/0.32	3.4
Bromobenzene	1.66/0.22	3.0
Toluene	1.48/0.17	2.7
4-Chlorophenol	0.45/−0.35	2.4
Phenol	0.26/−0.58	1.5
Pyrocatechol	0.14/−0.87	0.9
1a	1.88/0.27	3.44[d)]
1b	1.11/0.04	2.90[d)]
2a	3.99/0.60	4.22[d)]
2b	2.31/0.36	3.66[d)]
2c	0.02/−1.81	−1.51[d)]
3a	2.13/0.33	3.58[d)]
3b	1.19/0.07	2.97[d)]
3c	[e)]	[e)]

[a)] RP-HPLC analyses were performed at 25 °C using 0.1% aq. trifluoroacetic acid/CH_3CN (65:35) as mobile phase. [b)] Calculated with the equation $k = (t_R - t_0)/t_0$, where t_0 is the dead time (determined by injection of an unretained organic compound: uracil, t_0 = 0.58 min). [c)] Average values of three repeated injections. [d)] Calculated with the calibration (linear regression) equation: $\log P = (\log k + 1.175)/0.42$. [e)] An appropriate retention factor could not be obtained

for **3c** under the selected conditions due to its very fast elution from the column. Log *P* for this compound is then lower than –1.5, the value estimated for the less retained compound **2c**.

2.4. Live cell imaging studies.

To assess if this modular strategy could not only successfully modify the solubility properties of the tagged BODIPYs, but also ameliorate the lipophilicity and aggregation pitfalls that common BODIPYs usually present in biological applications, we have studied the behavior of the new dyes in live cell microscopy. To this end, live SCC38 cells (derived from human larynx squamous cell carcinoma) were incubated with aqueous solutions of **1a**-**b**, **2a**-**c**, and **3a**-**c** at different concentrations (50, 100 and 500 nM). The observed staining behavior depended on both, the structure of the chromophoric subunit and the tethered solubility module. For the same solubility module, fluorescence brightness decreased in the order **2a**-**b** > **3a**-**b** > **1a**-**b** (Figure 5), which, not surprisingly, is the same order observed in our prior photophysical study in water solution. In fact, fluorescent staining with **1a**-**b** was too weak to be of practical use even at the highest concentration assayed. Regarding the solubility module, no staining could be observed for BODIPYs tethered with double-charged sulfobetaines (**2c** and **3c**), which were not able to cross the cell membrane even after prolonged incubation, as recently observed for other dyes containing similar sulfobetaine substituents.[28] For the neutral BODIPYs, the longer the oligoethylene chain, the less cell-penetrating the BODIPY dye was. Thus, BODIPYs with the long octaethylene glycol chains (**2b** and **3b**) showed a weaker cell fluorescence signal, which could only be clearly observed for the larger and most lipophilic BODIPY **2b** at the highest concentration assayed (500 nM). In all cases, cell staining was rather diffuse, but some subcellular perinuclear reticulate staining pattern could still be observed that is consistent with partial nonspecific binding to the ER and Golgi for this series of dyes.

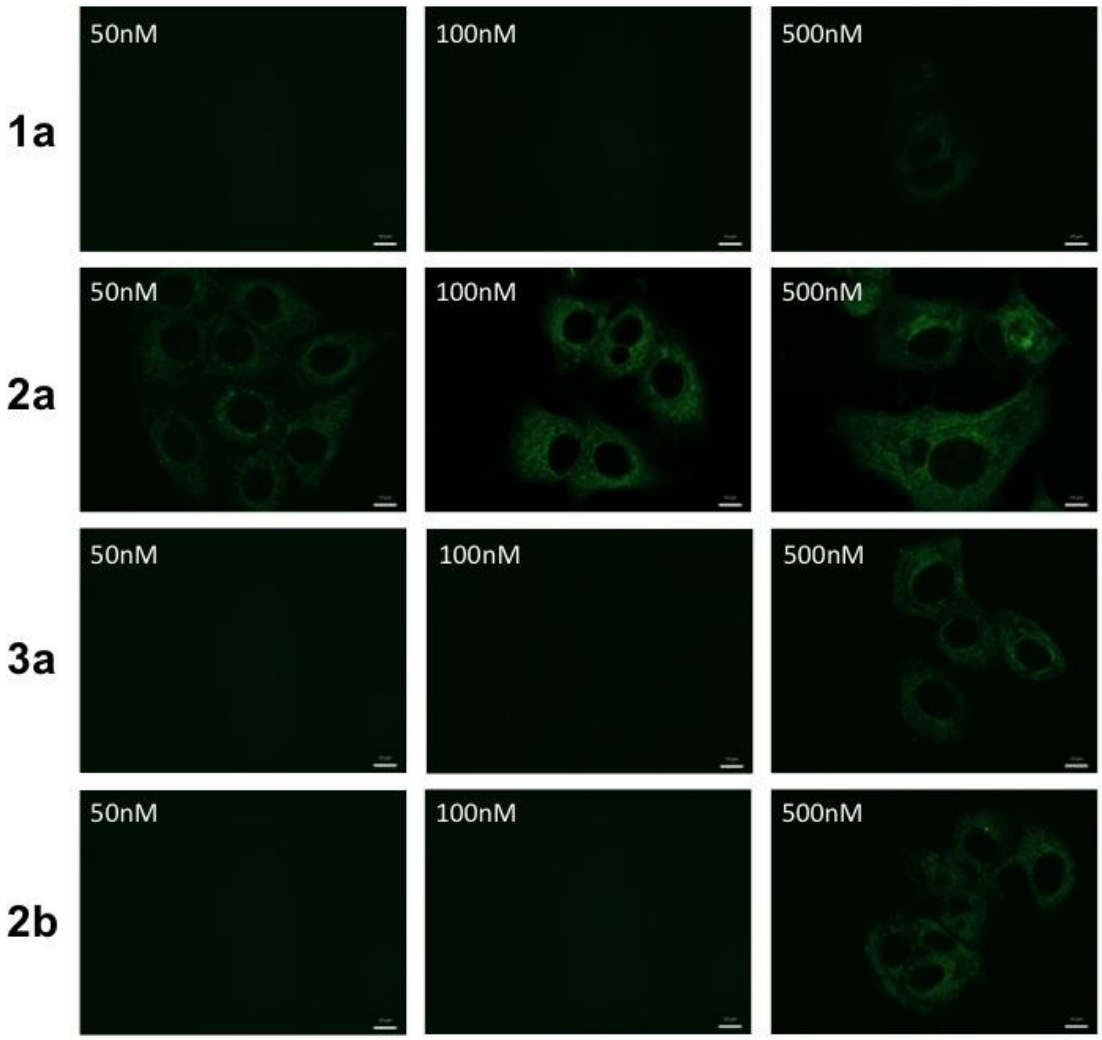

Figure 5. Representative fluorescence images and relative mean fluorescence intensities of live SCC38 cells incubated with the indicated concentrations of the new solubility-tagged *O*-BODIPYs for 30 min at 37 °C before washing and microscopic analysis. To compare fluorescence intensities for the different dyes and concentrations, all images were taken with the same exposure time (200 ms) on the same day. No staining could be observed for BODIPYs **2c** and **3c**, even at the highest concentration assayed (500 nM). Scale bars: 10 μm.

3. Conclusions

In this study, we have developed a modular one-pot synthetic strategy for the direct post-functionalization of *F*-BODIPYs with a structural subunit designed to fine-tune their solubility properties. This solubility module is based on a 2,4,6-trihydroxybenzoic acid scaffold onto which two solubility-tags are readily incorporated in three simple synthetic steps with good overall yield. The tethering reaction to the starting *F*-BODIPY dye uses easy-to-handle reagents, has broad functional group compatibility, and proceeds under mild conditions and in high yield without requiring any pre-functionalization of the chromophore, thus allowing the efficient incorporation of the solubility module at the end of the synthetic route without perturbing the chromophore scaffold. The orthogonal geometrical arrangement of this module with respect to the plane of the BODIPY chromophore hampers intermolecular aggregation processes that quench fluorescence. The covalent attachment of the module to the boron atom has a minimal effect on the absorption properties, while its effect on the fluorescence emission properties depends on the degree of alkylation of the chromophoric system. Thus, in the case of the non-alkylated chromophores derived from parent *F*-BODIPY **1**, low fluorescence quantum yields are observed due to deactivation by a thermodynamically facile ICT process, as predicted by DFT atomistic simulations. In comparison, alkylation of the BODIPY scaffold reduces its electron-acceptor character making any ICT process thermodynamically unfeasible and yielding highly efficient fluorescence, as observed for the dyes derived from *F*-BODIPYs **2** and **3**.

Fully water-soluble and hydrolytically stable BODIPYs have been prepared by incorporating hydrophilic chemical tags in the solubility module. The new water-soluble *O*-BODIPYs containing either neutral (tetra- and octa-ethylene glycol chains) or zwitterionic (sulfobetaine) tags are highly stable under the most common aqueous conditions used in biological settings (pH 6-8). Live cell imaging studies of the new dyes give very diffuse cell

staining with only minor subcellular perinuclear reticulate staining, attesting to their reduced lipophilicity as compared with typical BODIPY dyes. The observed cell membrane permeability depends on the nature and size of the chemical tags present in the solubility module, decreasing in the order: tetraethylene glycol > octaethylene glycol >> sulfobetaine. The new strategy can be readily adapted to the general and highly practical post-synthetic introduction of new functionalities into *F*-BODIPYs, including phase-tagging, by appropriately choosing the nature of the chemical tags attached to the module.

4. Experimental Section

4.1. General methods.

Proton and carbon-13 nuclear magnetic resonance (^{1}H NMR or ^{13}C NMR) spectra were recorded on a Bruker Avance III-400 (400 and 100 MHz, respectively) or a Varian System 500 (500 and 125 MHz, respectively) spectrometers. Chemical shifts are expressed in parts per million (δ scale) downfield from tetramethylsilane and are referenced to residual peaks of the deuterated NMR solvent used. Data are presented as follows: chemical shift, multiplicity (s = singlet, d = doublet, t = triplet, m = multiplet and/or multiple resonances, b = broad), integration, coupling constants in hertz (Hz), and assignment. Proton and carbon-13 assignments are based on gCOSY, gHSQC, and gHMBC correlation experiments. Thin layer chromatography (TLC) was performed with Merck Silica Gel 60 F254 plates and Merck Silica Gel 60 RP-18 F254S plates. Chromatograms were visualized using UV light (254 nm or 365 nm). Column chromatography was performed on a 971-FP Flash Purification System from Agilent Tecnologies using SF Si35 or C18 cartridges. High-resolution mass spectra (HRMS) were recorded on an Agilent 6520 Q-TOF instrument with an ESI source. Anhydrous solvents were prepared according to standard methods by distillation over drying agents or via elution through a PureSolv™ column drying system from Innovative Technology, Inc. All other solvents were of HPLC grade and were used as provided. All reactions were carried out with magnetic stirring and, if air or moisture

sensitive, in oven-dried glassware under argon. Microwave irradiation experiments were performed with a single-mode Anton Parr Monowave 300 reactor, using standard Pyrex tubes (10 mL capacity) sealed with a PTFE-lined rubber septum.

4.2. Synthesis of the solubility-tagged BODIPYs

*BODIPY **1a**.* A solution of *F*-BODIPY **1** (18.70 mg, 0.061 mmol), **7a** (33.30 mg, 0.061 mmol), and trimethylsilyl chloride (154 μL, 1.21 mmol) in dry acetonitrile (2.50 mL) was heated under microwave irradiation at 120 °C for 90 minutes. The solvent and excess volatile reagents were removed at reduced pressure and the resulting residue was purified by flash chromatography (CH_2Cl_2/MeOH 100:0 → 90:10) to afford **1a** (29 mg, 51%) as a red solid.

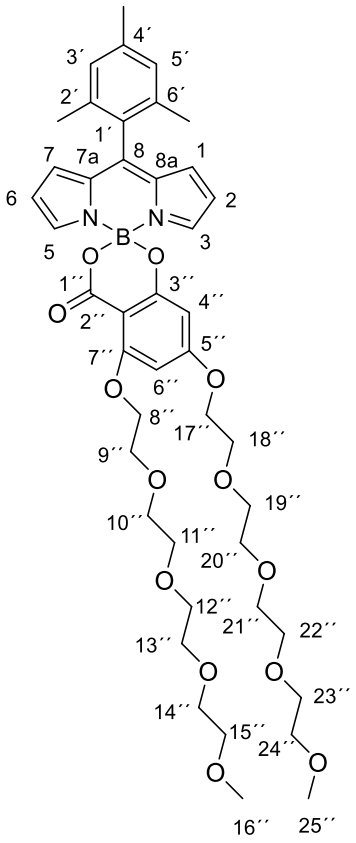

^{1}H NMR ($CDCl_3$, 400 MHz): δ = 7.69 (2H, s, H3 and H5), 6.95 (2H, s, H3′ and H5′), 6.68 (2H, d, *J* = 4.2 Hz, H1 and H7), 6.40 (2H, dd, *J* = 4.2, 1.9 Hz, H2 and H6), 6.16 (1H, d, *J* = 2.3 Hz, H6′′), 6.08 (1H, d, *J* = 2.3 Hz, H4′′), 4.22 (2H, t, *J* = 5.2 Hz, H8′′), 4.11 (2H, t, *J* = 4.7 Hz, H17′′), 3.99 (2H, t, *J* = 5.2 Hz, H9′′), 3.87 (2H, t, *J* = 4.7 Hz, H18′′), 3.84 (2H, br t, H10′′), 3.72-3.62 (18H, m, H11′′-H14′′ and H19′′-H23′′), 3.55-3.52 (4H, m, H24′′ and H15′′), 3.36 (3H, s, H16′′/H25′′), 3.36 (3H, s,

H25´´/H16´´), 2.36 (3H, s, $CH_3$4´), 2.14 (3H, s, $CH_3$2´/$CH_3$6´), 2.11 (3H, s, $CH_3$6´/$CH_3$2´). ^{13}C NMR ($CDCl_3$, 100 MHz): δ = 164.6 (C3´´), 162.3 (C7´´), 162.2 (C5´´), 160.8 (C1´´), 147.9 (C8), 144.7 (C3 and C5), 139.0 (C4´), 136.7 (C2´/C6´), 136.3 (C6´/C2´), 135.3 (C7a and C8a), 130.6 (C1 and C7), 129.7 (C1´), 128.4 (C3´/C5´), 128.2 (C5´/C3´), 118.8 (C2 and C6), 99.2 (C2´´), 95.6 (C4´´), 94.3 (C6´´), 72.1 (C15´´ and C24´´), 71.2 (C10´´), 71.0, 70.8, 70.8, 70.8, 70.8, 70.7, 70.7, 70.6, 70.6 (from 71.0 to 70.6: C11´´-C14´´ and C19´´-C23´´), 69.6 (C18´´), 69.4 (C9´´), 69.2 (C8´´), 67.7 (C17´´), 59.2 (C16´´/C25´´), 59.2 (C25´´/C16´´), 21.3 ($CH_3$4´), 20.3 ($CH_3$2´/$CH_3$6´), 20.2 ($CH_3$6´/$CH_3$2´). HRMS (API-ES$^+$) calcd. for $C_{43}H_{58}BN_2O_{13}$ $(M+H)^+$ 821.4034; found 821.4055; Calcd. for $C_{43}H_{57}BN_2NaO_{13}$ $(M+Na)^+$ 843.3853; found 843.3879.

*BODIPY **2a**.* A solution of *F*-BODIPY **2** (21.20 mg, 0.058 mmol), **7a** (26.20 mg, 0.048 mmol), and trimethylsilyl chloride (302 μL, 2.38 mmol) in dry acetonitrile (2.50 mL) was heated under microwave irradiation at 120 °C for 1 h. The solvent and excess volatile reagents were removed at reduced pressure and the resulting residue was purified by flash chromatography (CH_2Cl_2/MeOH 100:0 → 90:10) to afford **2a** (35.90 mg, 86%) as a red solid.

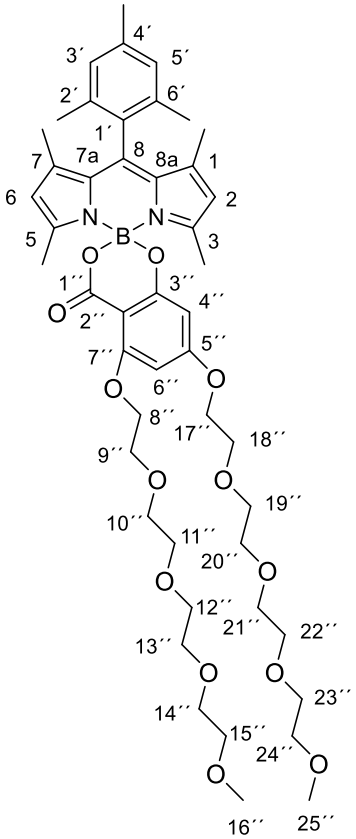

^{1}H NMR ($CDCl_3$, 400 MHz): δ = 6.95 (2H, s, H3′ and H5′), 6.10 (1H, d, *J* = 2.3 Hz, H6′′), 6.05 (1H, d, *J* = 2.3 Hz, H4′′), 5.92 (2H, s, H2 and H6), 4.19 (2H, t, *J* = 5.2 Hz, H8′′), 4.10 (2H, t, *J* = 4.9 Hz, H17′′), 3.98 (2H, t, *J* = 5.2 Hz, H9′′), 3.87-3.83 (4H, m, H10′′ and H18′′), 3.73-3.63 (18H, m, H11′′-H14′′ and H19′′-H23′′), 3.55-3.53 (4H, m, H15′′ and H24′′), 3.37 (3H, s, H16′′/H25′′), 3.36 (3H, s, H25′′/H16′′), 2.33 (3H, s, $CH_3$4′), 2.19 (6H, s, $CH_3$3 and $CH_3$5), 2.14 (3H, s, $CH_3$2′/$CH_3$6′), 2.11 (3H, s, $CH_3$6′/$CH_3$2′), 1.37 (6H, s, $CH_3$1 and $CH_3$7). ^{13}C NMR ($CDCl_3$, 100 MHz): δ = 164.7 (C7′′), 163.5 (C5′′), 162.2 (C1′′), 161.3 (C3′′), 155.8 (C3 and C5), 142.8 (C7a and C8a), 142.0 (C8), 138.8 (C4′), 135.3 (C2′/C6′), 134.9 (C2′/C6′), 131.3 (C1′), 131.2 (C1 and C7), 129.3 (C3′/C5′), 129.1 (C5′/C3′), 121.9 (C2 and C6), 99.7 (C2′′), 94.6 (C4′′), 93.7 (C6′′), 72.1 (C15′′/C24′′), 72.1 (C24′′/C15′′), 71.2 (C10′′), 71.0, 70.8, 70.8, 70.8, 70.7, 70.7, 70.6, 70.6 (from 71.0 to 70.6: C11′′-C14′′ and C19′′-C23′′), 69.6 (C18′′), 69.3 (C9′′), 69.1 (C8′′), 67.6 (C17′′), 59.2 (C16′′/C25′′), 59.2 (C25′′/C16′′), 21.3 ($CH_3$4′), 19.9 ($CH_3$2′/$CH_3$6′), 19.7 ($CH_3$6′/ $CH_3$2′), 15.5 ($CH_3$3 and $CH_3$5), 13.7 ($CH_3$1 and $CH_3$7). HRMS (API-ES$^+$) calcd. for $C_{47}H_{66}BN_2O_{13}$ $(M+H)^+$ 877.4660; found 877.4643; Calcd. for $C_{47}H_{65}BN_2NaO_{13}$ $(M+Na)^+$ 899.4480; found 899.4494.

*BODIPY **3a**.* A solution of *F*-BODIPY **3** (17.84 mg, 0.056 mmol), **7a** (32.73 mg, 0.059 mmol), and trimethylsilyl chloride (151 μL, 1.19 mmol) in dry acetonitrile (2.50 mL) was heated under microwave irradiation at 120 °C for 90 minutes. The solvent and excess volatile reagents were removed at reduced pressure and the resulting residue was purified by flash chromatography (CH_2Cl_2/MeOH 100:0 → 90:10) to afford **3a** (31.80 mg, 65%) as an orange solid.

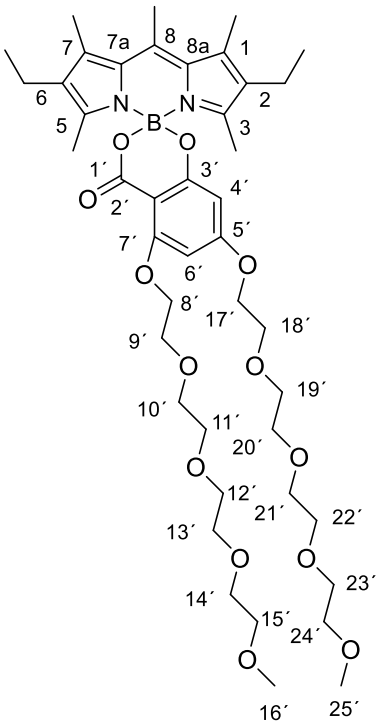

^{1}H NMR ($CDCl_3$, 400 MHz): δ = 6.09 (1H, d, *J* = 2.2 Hz, H6′), 6.00 (1H, d, *J* = 2.2 Hz, H4′), 4.18 (2H, t, *J* = 5.3 Hz, H8′), 4.08 (2H, t *J* = 4.7 Hz, H17′), 3.98 (2H, t, *J* = 5.3 Hz, H9′), 3.86-3.82 (4H, m, H10′ and H18′), 3.71-3.62 (18H, m, H11′′-H14′′ and H19′′-H23′′), 3.55-3.53 (4H, m, H15′ and H24′), 3.37 (3H, s, H16′/H25′), 3.36 (3H, s, H25′/ H16′), 2.62 (3H, s, $CH_3$8), 2.34 (4H, q, *J* = 7.5 Hz $CH_3\underline{CH_2}$2 and $CH_3\underline{CH_2}$6), 2.33 (3H, s, $CH_3$1/$CH_3$7), 2.32 (3H, s, $CH_3$7/$CH_3$1), 2.13 (6H, s, $CH_3$3 and $CH_3$5), 0.98 (6H, t, *J* = 7.5 Hz, $\underline{CH_3}CH_2$2 and $\underline{CH_3}CH_2$6). ^{13}C NMR ($CDCl_3$, 100 MHz): δ = 164.6 (C5′), 163.5 (C3′), 162.3 (C7′), 161.1 (C1′), 152.5 (C3 and C5), 140.0 (C8), 137.0 (C7a and C8a), 133.0 (C1 and C7), 132.4 (C2 and C6), 100.0 (C2′), 94.7 (C4′), 93.6 (C6′), 72.1 (C15′ and C24′), 71.2 (C10′), 71.0, 70.9, 70.8, 70.8, 70.7, 70.7 (from 71.0 to 70.7: C11′′-C14′′ and C19′′-C23′′), 69.6 (C18′), 69.4 (C9′), 69.1 (C8′), 67.6 (C17′), 59.2 (C16′/C25′), 59.2 (C25′/C16′), 17.4 ($CH_3$8), 17.3 ($CH_3\underline{CH_2}$2 and $CH_3\underline{CH_2}$6), 15.1 ($\underline{CH_3}CH_2$2 and $\underline{CH_3}CH_2$6), 14.7 ($CH_3$1 and $CH_3$7), 13.01 ($CH_3$3 and $CH_3$5). HRMS (API-ES$^+$) calcd. for $C_{43}H_{66}BN_2O_{13}$ $(M+H)^+$ 829.4660; found 829.4679; Calcd. for $C_{43}H_{65}BN_2NaO_{13}$ $(M+Na)^+$ 851.4479; found 851.4494.

*BODIPY **1b**.* A solution of *F*-BODIPY **1** (13.98 mg, 0.045 mmol), **7b** (37.0 mg, 0.045 mmol), and trimethylsilyl chloride (132 μL, 1.02 mmol) in dry acetonitrile (2.50 mL) was heated under microwave irradiation at 120 °C for 90 minutes. The solvent and excess volatile reagents were

removed at reduced pressure and the resulting residue was purified by flash chromatography (CH_2Cl_2/MeOH 100:0 → 90:10) to afford **1b** (35 mg, 72%) as a red solid.

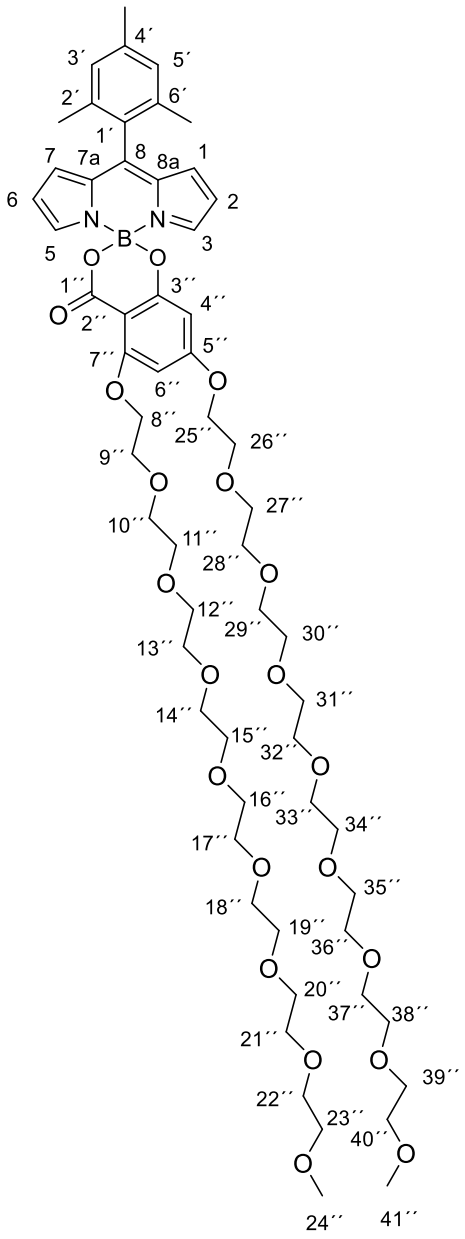

^{1}H NMR ($CDCl_3$, 400 MHz): δ = 7.69 (2H, s, H3 and H5), 6.96 (2H, s, H3′and H5′), 6.69 (2H, br d, H1 and H7), 6.41 (2H, dd, *J* = 4.2, 1.9 Hz, H2 and H6), 6.16 (1H, d, *J* = 2.2 Hz, H6′′), 6.09 (1H, d, *J* = 2.2 Hz, H4′′), 4.21 (2H, t, *J* = 5.1 Hz, H8′′), 4.11 (2H, t, *J* = 4.7 Hz, H25′′), 3.99 (2H, t, *J* = 5.1 Hz, H9′′), 3.90-3.82 (4H, m, H10′′ and H26′′), 3.73-3.62 (50H, m, H11′′-H22′′ and H27′′-H39′′), 3.58-3.53 (4H, m, H23′′ and H40′′) 3.37 (6H, s, H24′′ and H41′′), 2.36 (3H, s, $CH_3$4′), 2.14 (3H, s, $CH_3$2′/$CH_3$6′), 2.11(3H, s, $CH_3$6′/$CH_3$2′). ^{13}C NMR ($CDCl_3$, 100 MHz): δ = 164.6 (C5′′), 162.3 (C7′′), 162.2 (C3′′), 160.7 (C1′′), 147.9 (C8), 144.7 (C3 and C5), 139.0 (C4′), 136.7 (C2′/C6′),

136.3 (C6′/C2′), 135.3 (C7a and C8a), 130.6 (C1 and C7), 129.7 (C1′), 128.4 (C3′/C5′), 128.3 (C5′/C3′), 118.8 (C2 and C6), 99.2 (C2′′), 95.6 (C4′′), 94.3 (C6′′), 72.1 (C23′′ and C40′′), 71.3 (C10′′), 71.0, 70.9, 70.8, 70.8, 70.7, 70.7, 70.6 (from 71.9 to 70.6: C11′′-C22′′ and C27′′-C39′′), 69.6 (C26′′), 69.4 (C9′′), 69.2 (C8′′), 67.7 (C25′′), 59.2 (C24′′ and C41′′), 21.3 ($CH_3$4′), 20.3 ($CH_3$2′/$CH_3$6′), 20.2 ($CH_3$6′/$CH_3$2′). HRMS (API-ES$^+$) calcd. for $C_{59}H_{93}BN_3O_{21}$ $(M+NH_4)^+$ 1190.6399; found 1190.6362.

*BODIPY **2b**.* A solution of *F*-BODIPY **2** (24.54 mg, 0.067 mmol), **7b** (55.0 mg, 0.061 mmol), and trimethylsilyl chloride (197 µL, 1.52 mmol) in dry acetonitrile (2.50 mL) was heated under microwave irradiation at 120 °C for 45 minutes. The solvent and excess volatile reagents were removed at reduced pressure and the resulting residue was purified by flash chromatography (CH_2Cl_2/MeOH 100:0 → 70:30) to afford **2b** (35.90 mg, 80%) as a red solid.

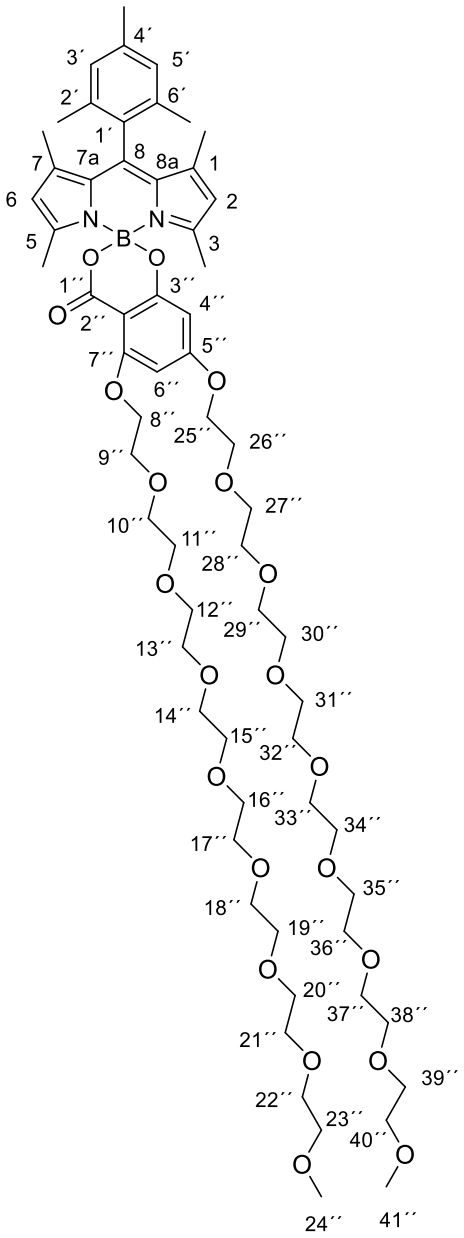

^{1}H NMR ($CDCl_3$, 400 MHz): δ = 6.95 (2H, s, H3′ and H5′), 6.09 (1H, d, *J* = 2.2 Hz, H6′′), 6.04 (1H, d, *J* = 2.2 Hz, H4′′), 5.92 (2H, s, H2 and H6), 4.18 (2H, t, *J* = 5.2 Hz, H8′′), 4.09 (2H, t, *J* = 4.7 Hz, H25′′), 3.98 (2H, t, *J* = 5.2 Hz, H9′′), 3.87-3.82 (4H, m, H26′′ and H10′′), 3.72-3.70 (2H, m, H27′′), 3.68-3.62 (48H, m, H11′′-H22′′ and H28′′-H39′′), 3.55-3.52 (4H, m, H23′′ and H40′′), 3.36 (6H, s, H24′′ and H41′′), 2.33 (3H, s, $CH_3$4′), 2.19 (6H, s, $CH_3$3 and $CH_3$5), 2.14 (3H, s, $CH_3$2′/$CH_3$6′), 2.10 (3H, s, $CH_3$6′/$CH_3$2′), 1.37 (6H, s, $CH_3$1 and $CH_3$7). ^{13}C NMR ($CDCl_3$, 100 MHz): δ = 164.7 (C5′′), 163.5 (C4′′), 162.2 (C7′′), 161.2 (C1′), 155.8 (C4 and C5), 142.8 (C7a and C8a), 142.0 (C8), 138.8 (C4′), 135.3 (C2′), 134.9 (C6′), 131.2 (C1/C7), 131.2 (C7/C1), 129.2 (C3′/C5′), 129.1 (C5′/C3′), 121.8 (C2 and C6), 99.7 (C2′′), 94.5 (C4′′), 93.7 (C6′′), 72.1 (C23′′ and C40′′), 71.2

(C10´´), 71.0 (C27´´), 70.8, 70.8, 70.7, 70.7, 70.6, 70.6 (from 70.8 to 70.6: C11´´-C22´´ and C28´´-C39´´) 69.6 (C26´´), 69.3 (C9´´), 69.2 (C8´´), 67.6 (C25´´), 59.2 (C24´´ and C41´´), 21.3 ($CH_3$4´), 19.8 ($CH_3$2´/$CH_3$6´), 19.7 ($CH_3$6´/$CH_3$2´), 15.5 ($CH_3$3 and $CH_3$5), 13.6 ($CH_3$1 and $CH_3$7). HRMS (API-ES$^+$) calcd. for $C_{63}H_{98}BN_2O_{21}$ $(M+H)^+$ 1229.6760; found 1229.6781.

*BODIPY **3b**.* A solution of *F*-BODIPY **3** (9.17 mg, 0.028 mmol), **7b** (26 mg, 0.028 mmol), and trimethylsilyl chloride (75 µL, 0.57 mmol) in dry acetonitrile (2 mL) was heated under microwave irradiation at 120 °C for 2 h. The solvent and excess volatile reagents were removed at reduced pressure and the resulting residue was purified by flash chromatography (CH_2Cl_2/MeOH 100:0 → 90:10) to afford **3b** (25 mg, 73%) as an orange solid.

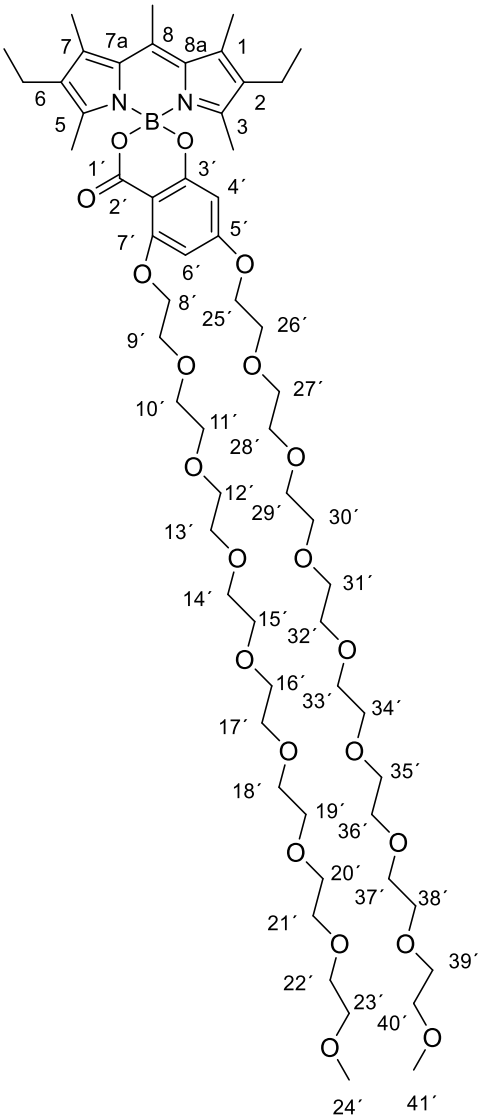

^{1}H NMR ($CDCl_3$, 500 MHz): δ = 6.09 (1H, d, *J* = 2.3 Hz, H6′), 6.00 (1H, d, *J* = 2.3 Hz, H4′), 4.17 (2H, t, *J* = 5.3 Hz, H8′), 4.08 (2H, t, *J* = 4.6 Hz, H25′), 3.98 (2H, t, *J* = 5.3 Hz, H9′), 3.86-3.82 (4H, m, H10′ and H26′), 3.72-3.70 (2H, m, H27′), 3.68-3.63 (48H, m, H11′-H22′ and H28′-H39′), 3.55-3.53 (4H, m, H23′ and H40′), 3.37 (6H, s, H24′ and H41′), 2.62 (3H, s, $CH_3$8), 2.35 (4H, q, *J* = 7.5 Hz, $CH_3\underline{CH_2}$2 and $CH_3\underline{CH_2}$6), 2.33 (6H, s, $CH_3$1 and $CH_3$7), 2.12 (6H, s, $CH_3$3 and $CH_3$5), 0.97 (6H, t, *J* = 7.5 Hz, $\underline{CH_3}CH_2$2 and $\underline{CH_3}CH_2$6). ^{13}C NMR ($CDCl_3$, 125 MHz): δ = 164.6 (C5′), 163.5 (C3′), 162.2 (C7′), 161.2 (C1′), 152.4 (C3 and C5), 140.0 (C8), 137.0 (C7a and C8a), 133.0 (C1 and C7), 132.4 (C2 and C6), 99.9 (C2′), 94.7 (C4′), 93.5 (C6′), 72.1 (C23′ and C40′), 71.2 (C10′), 71.0 (C27′), 70.8, 70.7, 70.7, 70.7, 70.6 (from 70.8 to 70.6: C11′-C22′ and C28′-C39′), 69.6 (C26′), 69.4 (C9′), 69.1 (C8′), 67.5 (C25′), 59.2 (C24′′ and C41′′), 17.4 ($CH_3$8), 17.2 ($CH_3\underline{CH_2}$2 and $CH_3\underline{CH_2}$6), 15.1 ($\underline{CH_3}CH_2$2 and $\underline{CH_3}CH_2$6), 14.7 ($CH_3$1 and $CH_3$7), 13.0 ($CH_3$3 and $CH_3$5). HRMS (API-ES$^+$) calcd. for $C_{59}H_{101}BN_3O_{21}$ $(M+NH_4)^+$ 1198.7025; found 1198.7024.

*BODIPY **2c**.* A suspension of *F*-BODIPY **2** (15 mg, 0.043 mmol), **7c** (20 mg, 0.031 mmol), and trimethylsilyl chloride (200 μL, 1.55 mmol) in dry acetonitrile (2 mL) was heated under microwave irradiation at 50 °C for 40 minutes, at 80 °C for 30 minutes, at 100 °C for 30 minutes, and at 120 °C for 30 minutes. The solvent and excess volatile reagents were removed at reduced pressure and the resulting residue was purified by reversed-phase column flash chromatography (H_2O/MeCN 100:0 → 0:100). The fractions containing product were combined and lyophilized to afford **2c** (16 mg, 53%) as a red solid.

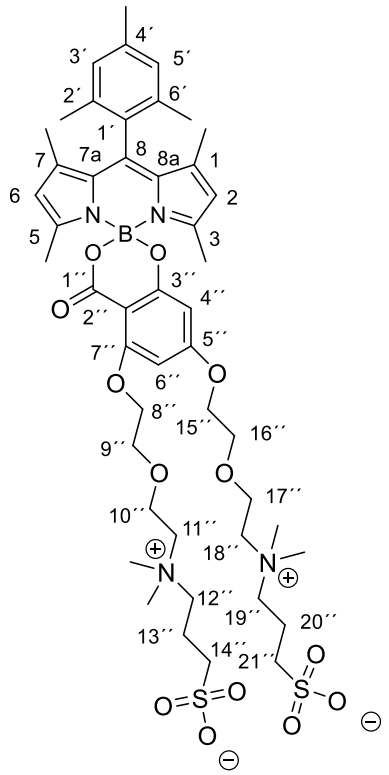

^{1}H NMR (CD_3OD, 400 MHz): δ = 7.08 (2H, s, H3′ and H5′), 6.26 (1H, d, *J* = 1.8 Hz, H4′′/H6′′), 6.18 (1H, d, *J* =1.8 Hz, H6′′/H4′′), 6.10 (2H, s, H2 and H6), 4.25-4.24 (4H, m, H8′′ and H15′′), 4.15 (2H, br m, H10′′/H17′′), 4.01 (2H, br m, H17′′/H10′′), 3.97 (2H, t, *J* = 3.9 Hz, H16′′/H9′′), 3.89 (2H, t, *J* = 3.9 Hz , H9′′/H16′′), 3.65-3.58 (8H, m, H11′′, H12′′, H18′′and H19′′), 3.18 (6H, s, $(CH_3)_2$N)), 3.18 (6H, s, $(CH_3)_2$N)), 2.85 (2H, t, *J* = 6.9 Hz, H14′′/H21′′), 2.73 (2H, t, *J* =6.9 Hz, H21′′/H14′′), 2.36 (3H, s, $CH_3$4′), 2.27-2.19 (4H, m, H13′′ and H20′′), 2.19 (6H, s, $CH_3$5 and $CH_3$6), 2.14 (3H, s, $CH_3$2′/$CH_3$6′), 2.11 (3H, s, $CH_3$6′/$CH_3$2′), 1.43 (6H, s, $CH_3$1 and $CH_3$7). ^{13}C NMR (CD_3OD, 100 MHz): δ = 167.1 (C3′′/C5′′/C7′′), 164.9 (C5′′/C7′′/C3′′), 164.4 (C7′′/C3′′/C5′′), 163.5 (C1′′), 157.1 (C3 and C5), 144.7 (C7a and C8a), 143.5 (C8), 140.7 (C4′), 135.9 (C2′ and C6′), 132.4 (C1 and C7), 132.2 (C1′), 130.4 (C3′ and C5′), 123.1 (C2 and C6), 99.5 (C2′′), 95.9 (C4′′/C6′′), 94.0 (C6′′/C4′′), 70.4 (C9′′/C16′′), 70.4 (C16′′/C9′′), 70.0 (C8′′/C15′′), 68.7 (C15′′/C8′′), 66.1 (C10′′/C17′′), 65.8 (C17′′/C10′′), 65.3 (C11′′/C12′′/C18′′/C19′′), 65.0 (C12′′/C18′′/C19′′/C11′′), 64.5 (C18′′/C19′′/C11′′/C12′′), 52.6 (2 × $(CH_3)_2$N), 48.7 (C14′′ and C21′′), 21.2 ($CH_3$4′), 20.1 (C13′′/C20′′), 20.1 (C20′′ and C13′′), 19.6 ($CH_3$2′/$CH_3$6′), 19.5

($CH_3$6′/ $CH_3$2′), 15.3 ($CH_3$3 and $CH_3$5), 13.7 ($CH_3$1 and $CH_3$7). HRMS (API-ES$^+$) calcd. for $C_{47}H_{66}BN_4O_{13}S_2$ $(M-H)^-$ 969.4174; found 969.4188.

*BODIPY **3c***. A suspension of *F*-BODIPY **3** (9.38 mg, 0.029 mmol), **7c** (19 mg, 0.029 mmol), and trimethylsilyl chloride (190 μL, 1.47 mmol) in dry acetonitrile (2 mL) was heated under microwave irradiation at 45 °C for 10 minutes, and at 50 °C for 50 minutes. The solvent and excess volatile reagents were removed at reduced pressure and the resulting residue was purified by reversed-phase C18 column chromatography (H_2O/MeCN 100:0 → 0:100). The fractions containing product were combined and lyophilized to afford **3c** (15.50 mg, 57%) as an orange solid.

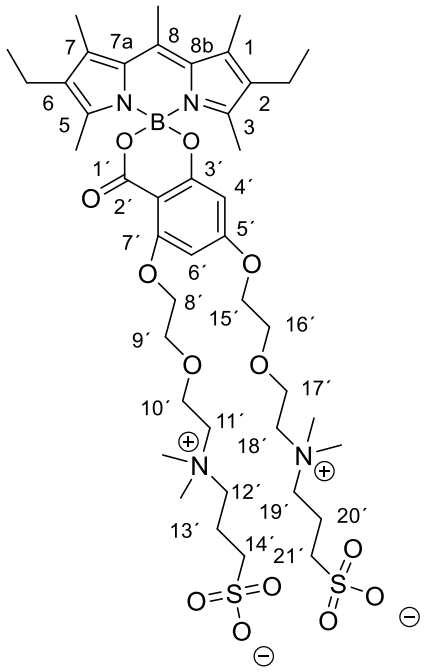

^{1}H NMR (CD_3OD, 400 MHz): δ = 6.24 (1H, d, *J* = 2.1 Hz, H4′/H6′), 6.10 (1H, d, *J* = 2.1 Hz, H6′/H4′), 4.23-4.20 (4H, m, H8′ and H15′), 4.14 (2H, br m, H10′/H17′), 4.00 (2H, br m, H17′/H10′), 3.96 (2H, t, *J* = 4.0 Hz, H9′/H16′), 3.87 (2H, t, *J* = 4.0 Hz, H16′/H9′) , 3.64-3.57 (8H, m, H11′, H12′, H18′and H19′), 3.18 (6H, s, $(CH_3)_2$N)), 3.17 (6H, s, $(CH_3)_2$N)), 2.84 (2H, t, *J* = 6.8 Hz, H14′/H21′), 2.75-2.71 (5H, m, $CH_3$8 and C21′/C14′), 2.44 (4H, q, *J* = 7.5 Hz, $CH_3\underline{CH_2}$2 and $CH_3\underline{CH_2}$6), 2.42 (3H, s, $CH_3$1/$CH_3$7), 2.41 (3H, s, $CH_3$7/$CH_3$1), 2.23-2.20 (4H, m, H13′ and H20′), 2.12 (6H, s, $CH_3$3 and $CH_3$5), 1.02 (6H, t, *J*= 7.5 Hz, $\underline{CH_3}CH_2$2 and $\underline{CH_3}CH_2$6). ^{13}C NMR (CD_3OD, 100 MHz): δ = 167.0

(C3′/C5′/C7′), 165.1 (C5′/C7′/C3′), 164.5 (C1′), 163.4 (C7′/C3′/C5′), 153.2 (C3 and C5), 142.5 (C7a and C8a), 139.2 (C8), 134.5 (C1 and C7), 133.6 (C2 and C6), 99.8 (C2′), 95.8 (C4′/C6′), 93.9 (C6′/C4′), 70.4 (C9′/C16′), 70.4 (C16′/C9′), 70.0 (C8′/C15′), 68.7 (C15′/C8′), 66.1 (C10′/C17′), 65.8 (C17′/C10′), 65.0 (C11′/C12′/C18′/C19′), 65.0 (C12′/C18′/C19′/C11′), 64.5 (C18′/C19′/C11′/C12′), 52.6 (2 × $(CH_3)_2N$), 48.7 (C14′ and C21′), 20.1 (C13′/C20′), 20.1 (C20′ and C13′), 17.8 ($CH_3\underline{CH_2}2$ and $CH_3\underline{CH_2}6$), 17.8 (CH_38), 15.3 ($\underline{CH_3}CH_22$ and $\underline{CH_3}CH_26$), 14.7 (CH_31 and CH_37), 13.0 (CH_33 and CH_35). HRMS (API-ES$^+$) calcd. for $C_{43}H_{68}BN_4O_{13}S_2$ $(M+H)^+$ 923.4319; found 923.4342.

4.3. Photophysical characterization

The photophysical properties for the new BODIPYs were measured in different solvents at low concentrations (approx. 2×10^{-6} M) in 1-cm optical path cuvettes. The UV/vis absorption spectra were recorded on a Varian dual beam spectrometer (CARY 7000) in transmittance mode. Emission spectra were recorded on an Edinburgh Instruments (FLSP920 model) spectrofluorimeter with a xenon flash lamp 450 W as the excitation source. The dependence of the fluorescence emission on the dye concentration was analyzed in front-face configuration using cuvettes of 1-mm optical path for concentrations ranging from *ca*. 5×10^{-6} M to 1×10^{-4} M or 0.1-mm optical path for concentrations higher than 2×10^{-4} M to match the optical density for each concentration range. The fluorescence spectra were corrected from the wavelength dependence of the detector sensibility. Fluorescence quantum yields (ϕ_{fl}) were obtained using as reference PM546 (ϕ_{fl} = 0.91) in cyclohexane or PM567 (ϕ_{fl} = 0.84) in ethanol. The fluorescence lifetime decay curves were measured with the time-correlated single-photon counting technique in the same spectrofluorimeter using a multichannel plate detector (Hamamatsu R38094–50) with picosecond time-resolution. Fluorescence decay curves were monitored at the maximum emission wavelength after excitation by means of a Fianium Supercontinuum laser with 150 ps full width at half maximum (FWHM) pulses. The fluorescence lifetime (τ) was

obtained after deconvolution of the instrumental response signal from the recorded decay curves by means of an iterative method. The goodness of the exponential fit was controlled by statistical parameters (chi-square, χ^2, and analysis of the residuals). The estimated error in the photophysical parameters measured in this work is of 10%.

4.4. Quantum mechanics calculations

Ground state geometries were optimized at the Density Functional Theory (DFT) using the hybrid B3LYP method, and the triple valence basis set with polarization and diffuse functions (6-311+G*). The energy minimization was carried out without any geometrical constraints and the geometries were considered as energy minimum when the corresponding frequency analysis did not give any negative value. The solvent effect (water) was considered in the conducted theoretical simulations by means of the Polarizable Continuum Model (PCM). All calculations were performed using the Gaussian 16 software as implemented in the computational cluster "Arina" of the UPV/EHU.

4.5. Log *P* determination.

Partition coefficients log *P* were indirectly determined by the RP-HPLC method.[25a] HPLC measurements were carried out on a Waters e2695 chromatographic system with a Waters 996 Photodiode Array UV−vis detector. The stationary phase was a C18 sunfire 3.5 μm 2.1 × 50 mm column. Mobile phase was 65% MeCN, 30% H_2O, and 5% H_2O containing 1% TFA. In brief, solutions of the reference compounds or of the new BODIPYs (*ca*. 100 μM) were repetitively injected in the column equilibrated with mobile phase at 0.35 mL/min. All measurements were made in triplicate. The t_0 for calculating the retention factor via $k = (t_R - t_0)/t_0$ was determined by using uracil as the unretained solute (t_0 = 0.557 min). The corresponding logarithms of the retention factors, log *k*, of the reference compounds were calculated and plotted as a function of the corresponding log *P* values reported in the literature using the shake-flask method (see Table 3). The partition coefficients of the BODIPY dyes could be interpolated from the corresponding logarithms of their retention factors, log *k*, using the calibration (linear

regression) equation: log P = (log k + 1.175)/0.42, obtained for the reference compounds (Figure S8 in Supplementary Material).

4.6. Live cell imaging studies

Cell culture. The established human squamous cell carcinoma (SCC38)-derived cell line was kindly provided by Dr. R. Grenman (University Central Hospital, Turku, Finland). SCC38 and HeLa cells were grown in DMEM supplemented with 10% fetal bovine serum, 100 units/mL penicillin, 200 μg/mL streptomycin, 2 mmol/L L-glutamine and 100 μmol/L nonessential amino acids. Cell lines were periodically tested for human pathogens and mycoplasma infection. All methods were carried out in accordance with the approved guidelines of our Institution.

Fluorescent cell labeling. Cells (50×10^3) were plated on black 24 well plates with flat and clear bottom suitable for fluorescence-based imaging of living cells (Ibidi GmbH) 24 hours before labeling. The new fluorescent probes were diluted in H_2O or DMSO, to a stock concentration of 500 μM, 100 μM or 50 μM. Adhered living cells were incubated with 500 nM, 100 nM, or 50 nM of probes, as indicated in figure legends, in DMEM without supplements for 30 minutes at 37 °C. Subsequently, the probes were removed and the cells were washed with PBS (3 × 5 min). Supplemented DMEM was then added to cells prior to microscopy analysis.

Live-cell microscopy. Microscopy imaging was performed on a Zeiss AxioObserver Z1 microscope (Carl Zeiss, Germany) with a Plan-Apochromat 40X/1.3 (NA = 1.3, working distance = 0.21 mm) or Plan-Apochromat 63X/1.4 (NA = 1.4, working distance = 0.19 mm) oil lens objective, a camera (AxioCam MRm; Carl Zeiss), and Apotome (ApoTome 2; Carl Zeiss).

Supplementary Material

Synthesis of the solubility tags, supplementary tables and figures, Cartesian coordinates and energies of all optimized structures, and copies of the ^1H and ^{13}C NMR spectra of all synthesized compounds.

Acknowledgements

We gratefully acknowledge the Spanish Ministerio de Economía y Competitividad (MINECO, projects MAT2017-83856-C3-1-P, MAT2017-83856-C3-3-P, and MAT2015-68837-REDT) and the Instituto de Salud Carlos III-Fondo de Investigación Sanitaria (CIBERONC) and Gobierno Vasco (IT912-16) for financial support. A. B.-M. and R. P. M. thank MINECO and UPV-EHU for a FPI predoctoral contract and predoctoral fellowship, respectively.

Received: ((will be filled in by the editorial staff))
Revised: ((will be filled in by the editorial staff))
Published online: ((will be filled in by the editorial staff))

ORCID:
Inmaculada García-Moreno: 0000-0002-8682-3715
Virginia Martínez-Martínez: 0000-0001-7551-3714
Jorge Bañuelos Prieto: 0000-0002-8444-4383
María D. Chiara: 0000-0002-1112-1583
Jose Luis Chiara: 0000-0002-8153-1852

References

[1] a) G. Ulrich, R. Ziessel, A. Harriman, *Angew. Chem. Int. Ed.* **2008**, 47, 1184; b) A. Loudet, K. Burgess, *Chem. Rev.* **2007**, 107, 4891; c) N. Boens, B. Verbelen, W. Dehaen, *Eur. J. Org. Chem.* **2015**, 2015, 6577; d) T. Kowada, H. Maeda, K. Kikuchi, *Chem. Soc. Rev.* **2015**, 44, 4953; e) J. Banuelos, *Chem. Rec.* **2016**, 16, 335; f) Y. S. Marfin, A. V. Solomonov, A. S. Timin, E. V. Rumyantsev, *Curr. Med. Chem.* **2017**, 24, 2745; g) S. Kolemen, E. U. Akkaya, *Coord. Chem. Rev.* **2018**, 354, 121; h) B. Bertrand, K. Passador, C. Goze, F. Denat, E. Bodio, M. Salmain, *Coord. Chem. Rev.* **2018**, 358, 108.

[2] a) F. Bergstroem, I. Mikhalyov, P. Haeggloef, R. Wortmann, T. Ny, L. B. A. Johansson, *J. Am. Chem. Soc.* **2002**, 124, 196; b) S. Cherumukkil, B. Vedhanarayanan, G. Das, V. K. Praveen, A. Ajayaghosh, *Bull. Chem. Soc. Jpn.* **2018**, 91, 100.

[3] L. P. Jameson, N. W. Smith, O. Annunziata, S. V. Dzyuba, *Phys. Chem. Chem. Phys.* **2016**, 18, 14182.

[4] a) O. Dilek, S. L. Bane, *Bioorg. Med. Chem. Lett.* **2009**, 19, 6911; b) T. Komatsu, Y. Urano, Y. Fujikawa, T. Kobayashi, H. Kojima, T. Terai, K. Hanaoka, T. Nagano, *Chem. Commun.* **2009**, 7015; c) T. Kowada, J. Kikuta, A. Kubo, M. Ishii, H. Maeda, S. Mizukami, K. Kikuchi,

J. Am. Chem. Soc. **2011**, 133, 17772; d) A. Romieu, C. Massif, S. Rihn, G. Ulrich, R. Ziessel, P.-Y. Renard, *New J. Chem.* **2013**, 37, 1016.

[5] a) T. Bura, R. Ziessel, *Org. Lett.* **2011**, 13, 3072; b) H. Xiong, H. Zuo, Y. Yan, G. Occhialini, K. Zhou, Y. Wan, D. J. Siegwart, *Adv. Mater.* **2017**, 29, 1700131.

[6] a) K. R. Gee, E. A. Archer, H. C. Kang, *Tetrahedron Lett.* **1999**, 40, 1471; b) N. J. Meltola, R. Wahlroos, A. E. Soini, *J. Fluoresc.* **2004**, 14, 635; c) J. Han, O. Gonzalez, A. Aguilar-Aguilar, E. Pena-Cabrera, K. Burgess, *Org. Biomol. Chem.* **2009**, 7, 34; d) L. Wu, A. Loudet, R. Barhoumi, R. C. Burghardt, K. Burgess, *J. Am. Chem. Soc.* **2009**, 131, 9156; e) S. L. Niu, C. Massif, G. Ulrich, R. Ziessel, P.-Y. Renard, A. Romieu, *Org. Biomol. Chem.* **2011**, 9, 66.

[7] a) S. C. Dodani, S. C. Leary, P. A. Cobine, D. R. Winge, C. J. Chang, *J. Am. Chem. Soc.* **2011**, 133, 8606; b) T. A. Prime, M. Forkink, A. Logan, P. G. Finichiu, J. McLachlan, P. B. L. Pun, W. J. H. Koopman, L. Larsen, M. J. Latter, R. A. J. Smith, M. P. Murphy, *Free Radical Biol. Med.* **2012**, 53, 544; c) K. Krumova, L. E. Greene, G. Cosa, *J. Am. Chem. Soc.* **2013**, 135, 17135; d) H. Yuan, H. Cho, H. H. Chen, M. Panagia, D. E. Sosnovik, L. Josephson, *Chem. Commun.* **2013**, 49, 10361; e) X. Zhang, C. Wang, Z. Han, Y. Xiao, *ACS Appl. Mater. Interfaces* **2014**, 6, 21669; f) X. Kong, F. Su, L. Zhang, J. Yaron, F. Lee, Z. Shi, Y. Tian, D. R. Meldrum, *Angew. Chem. Int. Ed.* **2015**, 54, 12053; g) S. Nigam, B. P. Burke, L. H. Davies, J. Domarkas, J. F. Wallis, P. G. Waddell, J. S. Waby, D. M. Benoit, A.-M. Seymour, C. Cawthorne, L. J. Higham, S. J. Archibald, *Chem. Commun.* **2016**, 52, 7114; h) B. Sui, S. Tang, A. W. Woodward, B. Kim, K. D. Belfield, *Eur. J. Org. Chem.* **2016**, 2016, 2851; i) X.-L. Liu, L.-Y. Niu, Y.-Z. Chen, M.-L. Zheng, Y. Yang, Q.-Z. Yang, *Org. Biomol. Chem.* **2017**, 15, 1072; j) X. Song, N. Li, C. Wang, Y. Xiao, *J. Mater. Chem. B* **2017**, 5, 360.

[8] a) Z. Li, T.-P. Lin, S. Liu, C.-W. Huang, T. W. Hudnall, F. P. Gabbai, P. S. Conti, *Chem. Commun.* **2011**, 47, 9324; b) I. Lopez-Duarte, T. T. Vu, M. A. Izquierdo, J. A. Bull, M. K. Kuimova, *Chem. Commun.* **2014**, 50, 5282; c) T. Papalia, G. Siracusano, I. Colao, A. Barattucci, M. C. Aversa, S. Serroni, G. Zappala, S. Campagna, M. T. Sciortino, F.

Puntoriero, P. Bonaccorsi, *Dyes Pigm.* **2014**, 110, 67; d) A. Poirel, P. Retailleau, A. De Nicola, R. Ziessel, *Chem. Eur. J.* **2014**, 20, 1252; e) D. Aydin Tekdas, G. Viswanathan, S. Zehra Topal, C. Y. Looi, W. F. Wong, G. Min Yi Tan, Y. Zorlu, A. G. Gurek, H. B. Lee, F. Dumoulin, *Org. Biomol. Chem.* **2016**, 14, 2665; f) K. Chansaenpak, H. Wang, M. Wang, B. Giglio, X. Ma, H. Yuan, S. Hu, Z. Wu, Z. Li, *Chem. Eur. J.* **2016**, 22, 12122; g) T. Gao, H. He, R. Huang, M. Zheng, F.-F. Wang, Y.-J. Hu, F.-L. Jiang, Y. Liu, *Dyes Pigm.* **2017**, 141, 530.

[9] a) S.-L. Niu, G. Ulrich, P. Retailleau, J. Harrowfield, R. Ziessel, *Tetrahedron Lett.* **2009**, 50, 3840; b) S. L. Niu, G. Ulrich, R. Ziessel, A. Kiss, P.-Y. Renard, A. Romieu, *Org. Lett.* **2009**, 11, 2049; c) S.-l. Niu, C. Massif, G. Ulrich, P.-Y. Renard, A. Romieu, R. Ziessel, *Chem. Eur. J.* **2012**, 18, 7229; d) J. Zhang, S. Zhu, L. Valenzano, F.-T. Luo, H. Liu, *RSC Adv.* **2013**, 3, 68.

[10] a) T. Uppal, N. V. S. D. K. Bhupathiraju, M. G. H. Vicente, *Tetrahedron* **2013**, 69, 4687; b) Z. Lu, L. Mei, X. Zhang, Y. Wang, Y. Zhao, C. Li, *Polym. Chem.* **2013**, 4, 5743; c) M. R. Martinez-Gonzalez, A. Urias-Benavides, E. Alvarado-Martinez, J. C. Lopez, A. M. Gomez, M. del Rio, I. Garcia, A. Costela, J. Banuelos, T. Arbeloa, I. Lopez Arbeloa, E. Pena-Cabrera, *Eur. J. Org. Chem.* **2014**, 2014, 5659; d) J. W. Fredy, J. Scelle, A. Guenet, E. Morel, S. Adam de Beaumais, M. Menand, V. Marvaud, C. S. Bonnet, E. Toth, M. Sollogoub, G. Vives, B. Hasenknopf, *Chem. Eur. J.* **2014**, 20, 10915; e) H. R. A. Golf, A. M. Oltmanns, D. H. Trieu, H.-U. Reissig, A. Wiehe, *Eur. J. Org. Chem.* **2015**, 2015, 4224; f) M. L. Lepage, A. Mirloup, M. Ripoll, F. Stauffert, A. Bodlenner, R. Ziessel, P. Compain, *Beilstein J. Org. Chem.* **2015**, 11, 659; g) N. Shivran, M. Tyagi, S. Mula, P. Gupta, B. Saha, B. S. Patro, S. Chattopadhyay, *Eur. J. Med. Chem.* **2016**, 122, 352; h) M. del Rio, F. Lobo, J. C. Lopez, A. Oliden, J. Banuelos, I. Lopez-Arbeloa, I. Garcia-Moreno, A. M. Gomez, *J. Org. Chem.* **2017**, 82, 1240; i) Q. Zhang, Y. Cai, Q.-Y. Li, L.-N. Hao, Z. Ma, X.-J. Wang, J. Yin, *Chem. Eur. J.* **2017**, 23, 14307; j) A. L. Nguyen, K. E. Griffin, Z. Zhou, F. R. Fronczek, K. M. Smith, M. G. H. Vicente, *New J. Chem.* **2018**, 42, 8241.

[11] Y. Liu, L.-Y. Niu, Y.-Z. Chen, Q.-Z. Yang, *J. Photochem. Photobiol. A* **2018**, 355, 311.

[12] T.-C. Chang, C.-T. Kuo, C.-C. Chiang, J.-Y. Cheng, C.-S. Yan, K. Peck, *Phys. Chem. Chem. Phys.* **1999**, 1, 3783.

[13] a) S. Atilgan, Z. Ekmekci, A. L. Dogan, D. Guc, E. U. Akkaya, *Chem. Commun.* **2006**, 4398; b) S. Zhu, J. Zhang, G. Vegesna, F.-T. Luo, S. A. Green, H. Liu, *Org. Lett.* **2011**, 13, 438; c) M. Isik, T. Ozdemir, I. S. Turan, S. Kolemen, E. U. Akkaya, *Org. Lett.* **2013**, 15, 216; d) G. Fan, L. Yang, Z. Chen, *Front. Chem. Sci. Eng.* **2014**, 8, 405; e) A. M. Courtis, S. A. Santos, Y. Guan, J. A. Hendricks, B. Ghosh, D. M. Szantai-Kis, S. A. Reis, J. V. Shah, R. Mazitschek, *Bioconjugate Chem.* **2014**, 25, 1043.

[14] a) H. Manzano, I. Esnal, T. Marques-Matesanz, J. Banuelos, I. Lopez-Arbeloa, M. J. Ortiz, L. Cerdan, A. Costela, I. Garcia-Moreno, J. L. Chiara, *Adv. Funct. Mater.* **2016**, 26, 2756; b) A. Blazquez-Moraleja, L. Cerdan, I. Garcia-Moreno, E. Avellanal-Zaballa, J. Banuelos, M. L. Jimeno, I. Lopez-Arbeloa, J. L. Chiara, *Chem. Eur. J.* **2018**, 24, 3802.

[15] R. G. Dushin, S. J. Danishefsky, *J. Am. Chem. Soc.* **1992**, 114, 655.

[16] O. Mitsunobu, *Synthesis* **1981**, 1.

[17] D. Du, J. Cai, H. Ju, F. Yan, J. Chen, X. Jiang, H. Chen, *Langmuir* **2005**, 21, 8394.

[18] W. W. Kaeding, *J. Org. Chem.* **1964**, 29, 2556.

[19] a) C. Tahtaoui, C. Thomas, F. Rohmer, P. Klotz, G. Duportail, Y. Mély, D. Bonnet, M. Hibert, *J. Org. Chem.* **2007**, 72, 269; b) X.-D. Jiang, J. Zhang, T. Furuyama, W. Zhao, *Org. Lett.* **2012**, 14, 248; c) T. Lundrigan, S. M. Crawford, T. S. Cameron, A. Thompson, *Chem. Commun.* **2012**, 48, 1003; d) G. Duran-Sampedro, A. R. Agarrabeitia, L. Cerdan, M. E. Perez-Ojeda, A. Costela, I. Garcia-Moreno, I. Esnal, J. Banuelos, I. L. Arbeloa, M. J. Ortiz, *Adv. Funct. Mater.* **2013**, 23, 4195; e) A. L. Nguyen, P. Bobadova-Parvanova, M. Hopfinger, F. R. Fronczek, K. M. Smith, M. G. H. Vicente, *Inorg. Chem.* **2015**, 54, 3228; f) G. Zhang, M. Wang, F. R. Fronczek, K. M. Smith, M. G. H. Vicente, *Inorg. Chem.* **2018**, 57, 14493.

[20] G. Duran-Sampedro, A. R. Agarrabeitia, I. Garcia-Moreno, L. Gartzia-Rivero, S. de la Moya, J. Banuelos, I. Lopez-Arbeloa, M. J. Ortiz, *Chem. Commun.* **2015**, 51, 11382.

[21] a) F. Lopez Arbeloa, T. Lopez Arbeloa, I. Lopez Arbeloa, I. Garcia-Moreno, A. Costela, R. Sastre, F. Amat-Guerri, *Chem. Phys.* **1998**, 236, 331; b) A. Costela, I. Garcia-Moreno, C. Gomez, R. Sastre, F. Amat-Guerri, M. Liras, F. Lopez Arbeloa, J. Banuelos Prieto, I. Lopez Arbeloa, *J. Phys. Chem. A* **2002**, 106, 7736.

[22] H. L. Kee, C. Kirmaier, L. Yu, P. Thamyongkit, W. J. Youngblood, M. E. Calder, L. Ramos, B. C. Noll, D. F. Bocian, W. R. Scheidt, R. R. Birge, J. S. Lindsey, D. Holten, *J. Phys. Chem. B* **2005**, 109, 20433.

[23] a) S. Shaban Ragab, S. Swaminathan, E. Deniz, B. Captain, F. M. Raymo, *Org. Lett.* **2013**, 15, 3154; b) P. Stachelek, A. A. Alsimaree, R. B. Alnoman, A. Harriman, J. G. Knight, *J. Phys. Chem. A* **2017**, 121, 2096; c) C. Ray, L. Diaz-Casado, E. Avellanal-Zaballa, J. Banuelos, L. Cerdan, I. Garcia-Moreno, F. Moreno, B. L. Maroto, I. Lopez-Arbeloa, S. de la Moya, *Chem. Eur. J.* **2017**, 23, 9383; d) L. Gartzia-Rivero, E. M. Sanchez-Carnerero, J. Jimenez, J. Banuelos, F. Moreno, B. L. Maroto, I. Lopez-Arbeloa, S. de la Moya, *Dalton Trans.* **2017**, 46, 11830.

[24] I. Lopez Arbeloa, *J. Photochem.* **1980**, 14, 97.

[25] a) D. J. Minick, J. H. Frenz, M. A. Patrick, D. A. Brent, *J. Med. Chem.* **1988**, 31, 1923; b) J. Sangster, *J. Phys. Chem. Ref. Data* **1989**, 18, 1111.

[26] C. A. Lipinski, F. Lombardo, B. W. Dominy, P. J. Feeney, *Adv. Drug Delivery Rev.* **2001**, 46, 3.

[27] a) R. Saito, A. Ohno, E. Ito, *Tetrahedron* **2010**, 66, 583; b) J. Wang, Y. Hou, W. Lei, Q. Zhou, C. Li, B. Zhang, X. Wang, *ChemPhysChem* **2012**, 13, 2739; c) D. Lhenry, M. Larrouy, C. Bernhard, V. Goncalves, O. Raguin, P. Provent, M. Moreau, B. Collin, A. Oudot, J.-M. Vrigneaud, F. o. Brunotte, C. Goze, F. Denat, *Chem. Eur. J.* **2015**, 21, 13091; d) J. H. Gibbs, Z. Zhou, D. Kessel, F. R. Fronczek, S. Pakhomova, M. G. a. H. Vicente, *J. Photochem. Photobiol. B: Biology* **2015**, 145, 35; e) J. C. Er, C. Leong, C. L. Teoh, Q. Yuan, P. Merchant, M. Dunn, D. Sulzer, D. Sames, A. Bhinge, D. Kim, S.-M. Kim, M.-H. Yoon, L. W. Stanton, S. H.

Je, S.-W. Yun, Y.-T. Chang, *Angew. Chem. Int. Ed.* **2015**, 54, 2442 ; f) S. Xuan, N. Zhao, Z. Zhou, F. R. Fronczek, M. G. a. H. Vicente, *J. Med. Chem.* **2016**, 59, 2109 ; g) S. Nigam, B. P. Burke, L. H. Davies, J. Domarkas, J. F. Wallis, P. G. Waddell, J. S. Waby, D. M. Benoit, A.-M. Seymour, C. Cawthorne, L. J. Higham, S. J. Archibald, *Chem. Commun.* **2016**, 52, 7114 ; h) K. Chansaenpak, H. Wang, M. Wang, B. Giglio, X. Ma, H. Yuan, S. Hu, Z. Wu, Z. Li, *Chem. Eur. J.* **2016**, 22, 12122 ; i) D. Aydin Tekda, G. Viswanathan, S. Zehra Topal, C. Y. Looi, W. F. Wong, G. Min Yi Tan, Y. Zorlu, A. e. G. l. G?rek, H. B. Lee, F. Dumoulin, *Org. Biomol. Chem.* **2016**, 14, 2665 ; j) J. M. Zimbron, K. v. Passador, B. Gatin-Fraudet, C.-M. Bachelet, D. Plazuk, L.-M. Chamoreau, C. Botuha, S. Thorimbert, M. l. Salmain, *Organometallics* **2017**, 36, 3435

[28] P. Shieh, V. T. Dien, B. J. Beahm, J. M. Castellano, T. Wyss-Coray, C. R. Bertozzi, *J. Am. Chem. Soc.* **2015**, 137, 7145.

"Click-type" solubility-tagging, a general and practical post-synthetic strategy for the one-step functionalization of *F*-BODIPYs with a structural subunit designed to fine-tune their solubility properties. The solubility module, based on a 2,4,6-trihydroxybenzoic acid scaffold (red) incorporating two solubility-tags (blue), is readily attached to the boron atom using easy-to-handle reagents. The tagged dyes show reduced lipophilicity, increased water-solubility and high stability towards hydrolysis.

Fluorescent dyes

A. Blázquez-Moraleja, D. Álvarez-Fernández, R. Prieto Montero, I. García-Moreno, V. Martínez-Martínez,* J. Bañuelos Prieto, I. Sáenz-de-Santa-María, M. D. Chiara, and J. L. Chiara*

A General Modular Approach for the Solubility Tagging of BODIPY Dyes

ToC figure: